

X-ray Detectors IV

Silicon will Rule the Planet

Sol M. Gruner

Physics Dept. & Cornell High Energy Synchrotron Source (CHESS)

Cornell University

Ithaca, NY 14853

smg26@cornell.edu



Direct Detection in Semiconductors

[Ref: Bertolini & Coche, eds., *Semiconductor Detectors* (North-Holland, Amsterdam, 1968)]

Within about 1 ns an absorbed x-ray in solid matter results in many electron-hole (e-h) pairs. This is a very localized process since the range of low energy electrons is very short in most materials:

$$\begin{aligned} R &= 0.090 \rho^{-0.8} E^{1.3} && \text{for } E < 10 \text{ keV} \\ R &= 0.045 \rho^{-0.9} E^{1.7} && \text{for } E > 10 \text{ keV,} \end{aligned}$$

where R (microns) is the thickness of material to reduce the electron transmission to 1%, E is the electron kinetic energy (keV) and ρ is the material density (g cm^{-3}). For Si & 10 keV x-rays, $R \approx 1 \mu\text{m}$.

The mean number of e-h pairs/x-ray of energy E is $N_{eh} = E / \varepsilon$,

where $\varepsilon \equiv$ mean ionization energy to produce an e-h pair. Typically, ε is a few eV, so many e-h pairs result. Furthermore, the fractional variation, $\sigma(N_{eh}) / N_{eh}$, in the number produced is quite small because the energy degradation process offers few channels which do not lead to electron-hole pairs:

$$\sigma(N_{eh}) / N = \sigma(E) / E = \sqrt{F\varepsilon / E} = \sqrt{F / N_{eh}},$$

where F is an empirical factor known as the Fano factor. For Si, $F \approx 0.1$, which is why semiconductor detectors have excellent energy resolution.



Semiconductor Detectors

Klein's empirical formula relates energy, E , to create electron-hole pair to the band gap:

$$E = 2.67 E_{gap} + 0.87,$$

where E_{gap} = energy band gap in the semiconductor.

Table 1
Physical characteristics of the semiconductors

Semi-conductor	ρ [g/cm ³]	Z	E_{gap} [eV]	ϵ [eV]	$T_{working}$ [K]	K-edge [keV]	ρ_c [Ω cm]	$\mu_{e,h}, \tau_{e,h}$ [cm ² /V]
Si	2.33	14	1.12	3.6 [1]	300	1.8	$\approx 10^3$	0.42, 0.22
Ge	5.33	32	0.67	2.9 [3]	77	11.1	$\approx 10^2$	0.72, 0.84
GaSe	4.55	31, 34	2.03	4.5 [4]	300	10.3, 12.6		$10^{-7}, 10^{-7}$ $1.5 \times 10^{-6}, 2.5 \times 10^{-6}$
InP	4.78	49, 15	1.30	4.2 [6]	300	27.9, 2.1	$\approx 10^7$	$4.8 \times 10^{-6}, \leq 10^{-7}$
CdS	4.84	48, 16	2.60	7.3 [15]	300	26.7, 2.4		
GaAs	5.32	31, 33	1.43	4.3 [3]	300	10.3, 11.8	$\approx 10^7$	$8.6 \times 10^{-6}, 4.0 \times 10^{-7}$ $8.6 \times 10^{-5}, 4.0 \times 10^{-6}$
InSb	5.77	49, 51	0.20	0.6 [15]	4	27.9, 30.4		$10^{-5}, 7.5 \times 10^{-6}$
CdSe	5.80	48, 34	1.73	5.5 ^a	300	26.7, 12.6		$2.0 \times 10^{-5}, 1.5 \times 10^{-6}$
CdTe	6.20	48, 52	1.44	4.7 [3]	300	26.7, 31.8	$\approx 10^9$	$2.0 \times 10^{-3}, 4.0 \times 10^{-4}$
PbI ₂	6.20	82, 53	2.55	7.7 ^a	300	88.0, 33.2	$> 10^{13}$	$8.0 \times 10^{-6}, 2.0 \times 10^{-7}$
HgI ₂	6.40	80, 53	2.13	4.2 [7]	300	83.1, 33.2	10^{13}	$10^{-4}, 10^{-5}$
TlBr	7.56	81, 35	2.68	6.5 [18]	300	85.5, 13.5	$\approx 10^{12}$	$1.6 \times 10^{-5}, 1.5 \times 10^{-6}$

^a Calculated from Klein's empirical formula [4].

Bencivelli, et al, Nuc. Instr. Meth. Phys. Res. A310 (1991) 210-214.



Semiconductor Detectors

Electron-hole pairs rapidly recombine unless swept apart, such as in the depletion zone of semiconductor diode. The behavior of electrons and holes in the depletion zone determine the x-ray detecting characteristics of the semiconductor. One type of depletion zone is the surface barrier (Schottky) type, which forms at the junction of a semiconductor and a suitable metal:

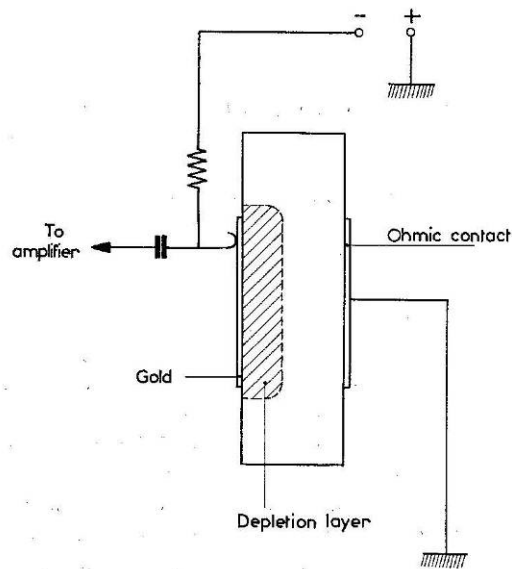


Fig. 2.2.1. Schematic representation of a surface barrier detector (generally gold - N-type silicon).

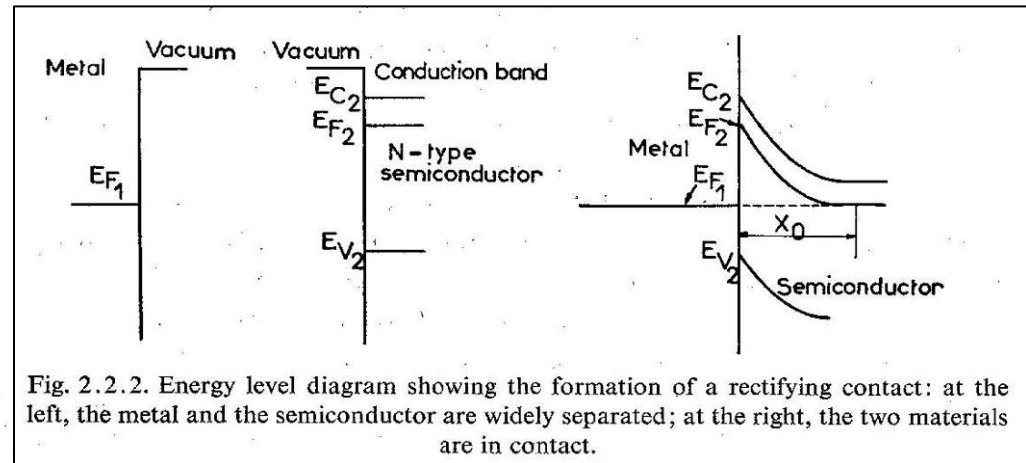


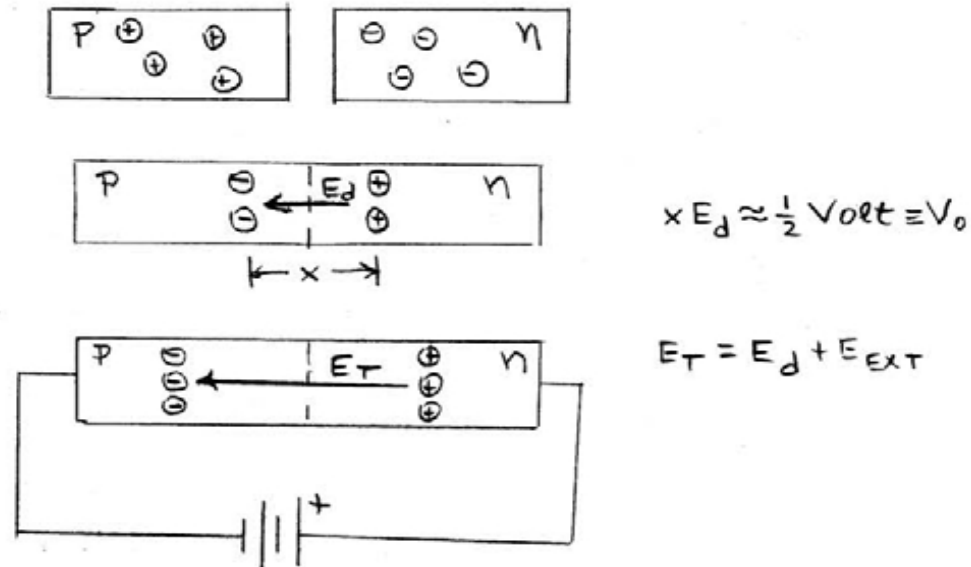
Fig. 2.2.2. Energy level diagram showing the formation of a rectifying contact: at the left, the metal and the semiconductor are widely separated; at the right, the two materials are in contact.

Bertolini & Coche, eds., *Semiconductor Detectors* (North-Holland, Amsterdam, 1968). pg 132.



Semiconductor Detectors

The n-p junction type of depletion zone is more important:



Imagine a p-n junction. Initially each material is charge neutral, the main difference between them being that the n-type material effectively has only electrons as mobile charge carriers with the charge-compensating holes fixed in the lattice, while the p-type material is the other way around. The mobile carriers may be considered to be a kind of gas of charged particles diffusing about fixed counterparts of the opposite electrical sign. When the two types of material are brought into contact at room temperature, the electrons diffuse across the junction into the p material and the holes diffuse across into



Semiconductor Detectors

the n-material. In doing so, however, charge neutrality in each material is violated. The p material now has a surplus of electrons and the n material a surplus of holes, thereby creating an electric field which points from n to the p material. At equilibrium, the electric field strength is sufficient to prevent further net separation of holes and electrons. Call the resultant net potential across the junction V_0 ; it is a function of the temperature and the properties of the materials. A consequence of the field is that any mobile charges introduced into the field region are swept, depending on their sign, toward one end or another of the region; hence, the region is depleted of free charge carriers and is known as the depletion zone. Since the depletion zone has no free charge carriers, it effectively is an insulating gap. It is readily shown that the width of the depletion zone is given by

$$x = \left[\frac{2\varepsilon V_0}{e} \cdot \frac{(N_a + N_d)}{N_a N_d} \right]^{\frac{1}{2}},$$

where ε is the semiconductor dielectric constant, e is the magnitude of charge of the electron, and N_a and N_d are the bulk concentrations of acceptor and donor dopants in the p and n-type materials, respectively.

If the n and p sides of the junction are now connected to the positive and negative terminals, respectively, of a battery then there is an additional component of electric field across the junction which adds to the contact field, displaces the equilibrium separation of charge and expands the width of the depletion zone. The junction is now reverse-biased.



Semiconductor Detectors

Typically, one material, say the p-type, is much more heavily doped than the other, in which case $N_a \gg N_d$, and the imposed potential $V \gg V_o$. In this case

$$x \approx \sqrt{2\epsilon\mu_n\rho_nV} ,$$

where μ_n is the electron mobility and ρ_n is the resistivity of the n-type material. Consequently, for a thick depletion zone, which is desired for an x-ray detector, one needs some combination of a high imposed potential, high resistivity, or high electron mobility. A analogous equation holds if the n-type material is more heavily doped.

If an x-ray stops in the depletion zone the electron hole pairs which are created are swept to the respective ends of the diode and appear as a current pulse. Since the number of electron-hole pairs is ideally proportional to the x-ray energy, the charge of the pulse is proportional to the x-ray energy.



Semiconductor Detectors

In order to be useful as a quantitative x-ray converter, the semiconductor detector should ideally meet many constraints:

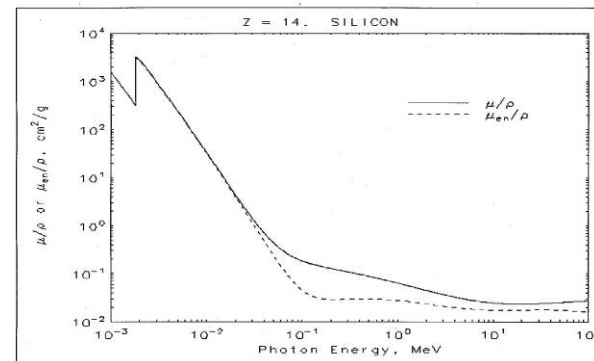
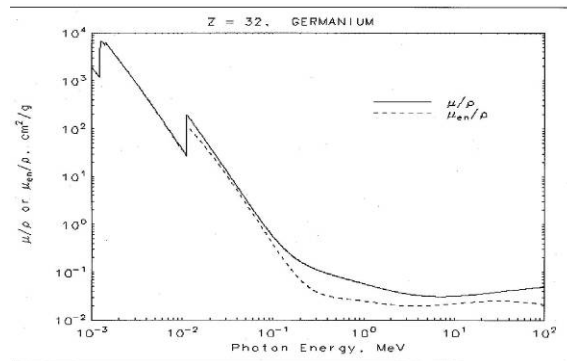
- The width of the material between the depletion zone and the incident x-rays should be thin, since x-rays which are stopped in these regions do not contribute to the signal.
- The depletion zone should have high stopping power, so high-Z semiconductors are attractive.
- The rate of loss of the dominant signal carriers (i.e., electrons in the above example) should be low. Carriers may be lost through recombination or trapping.
- Spontaneous generation of electron-hole pairs should be low, since these constitute a dark current in the absence of x-rays. Electron-hole pairs may be created thermally or at various defects, especially at the interfaces of the device.
- The junction capacitance should be as low as possible, since, in general, the performance of the charge sensitive preamplifier connected to the detector degrades with increasing input capacitance.
- The Fano factor of the semiconductor should be as low as possible for low noise performance.
- The detector should be robust, stable, of adequate size, etc.
- Most importantly, good quality semiconductor material, and the techniques to fabricate it, must be available.



Semiconductor Detectors

Not surprisingly, the availability of high quality semiconductor is directly linked to its use by the electronics industry. Silicon is nearly ideal in all respects except for stopping power considerations.

The figures below show the attenuation coefficient of Si and Ge. The attenuation coefficient of Si falls from 33.9 cm²/g at 10 keV to 4.5 cm²/g at 20 keV. Germanium (42.2 cm²/g) and gallium arsenide are both still effective at 20 keV, but large area, high quality, high resistivity materials are more difficult to obtain than with silicon. Other semiconductors (e.g., HgI₂, TlBr, etc.) have high attenuation coefficients but are even more difficult to obtain at acceptable quality.



By the equations given above, the depletion layer thickness $x \sim \sqrt{V\rho}$. But it is difficult to obtain Si with resistivities $> 10\text{k } \Omega\text{cm}$. Voltages are also limited by breakdown, so in practice, depletion zones of p-n junctions are limited to about 1.5mm. This is far too thin for many applications.



Si(Li) & Ge(Li) Drifted Detectors

A method to increase the depletion zone thickness of p-type material is to use high voltage and temperature to drift in Li ions. When the temperature is lowered, the Li atoms act as donors which compensate for the holes, thereby allowing near-intrinsic resistivities. Drifting the proper distribution of Li atoms is an art, but resistivities on the order of $100\text{k } \Omega\text{cm}$ have been achieved, allowing effective depletion thicknesses of 1 – 2 cm. Because the drifted region approaches intrinsic resistivities, the junction is often called a PIN junction. At cryogenic temperatures, these detectors have stable characteristics and very low noise, even for relatively large areas.

The resultant lithium drifted Si or Ge diodes have exceptionally thick depletion zones and low noise, making Si(Li) and Ge(Li) counters suitable for energy-discriminating detectors at high x-ray energies.

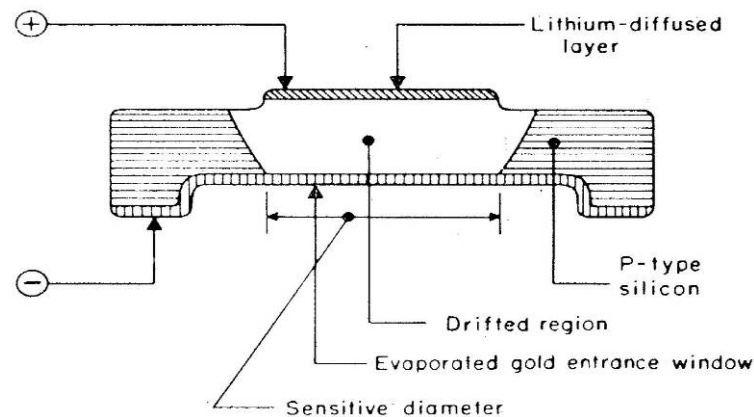


Fig. 2.3.9. High-voltage lithium drifted silicon detector.

Bertolini & Coche, eds., *Semiconductor Detectors* (North-Holland, Amsterdam, 1968).



Silicon Drift Detectors

The depletion zones described so far usually have an electric field which, barring edge effects, points straight across the junction. In 1984 Gatti and Rehak pointed out that the field may be shaped by a voltage gradient on electrodes on a face of the junction, allowing carriers to be funneled to a collection point. An example of the diode geometry and the corresponding potential is shown:

P. Lechner et al. / Nucl. Instr. and Meth. in Phys. Res. A 377 (1996) 346–351

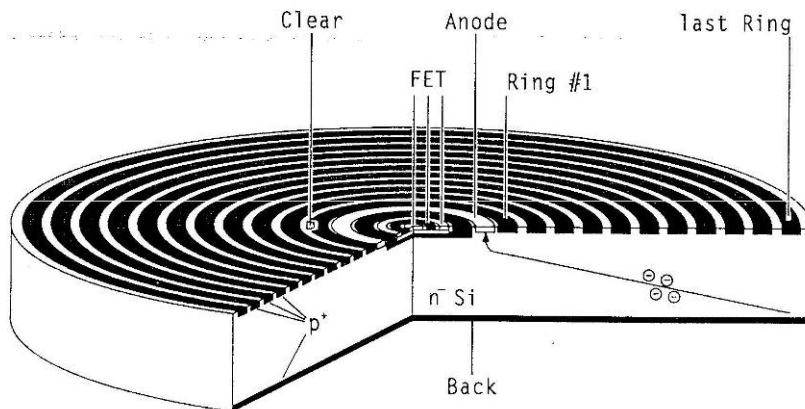


Fig. 1. Cross section of a cylindrical silicon drift detector with integrated n-channel JFET. The gate of the transistor is connected to the collecting anode. The radiation entrance window for the ionizing radiation is the non-structured backside of the device.

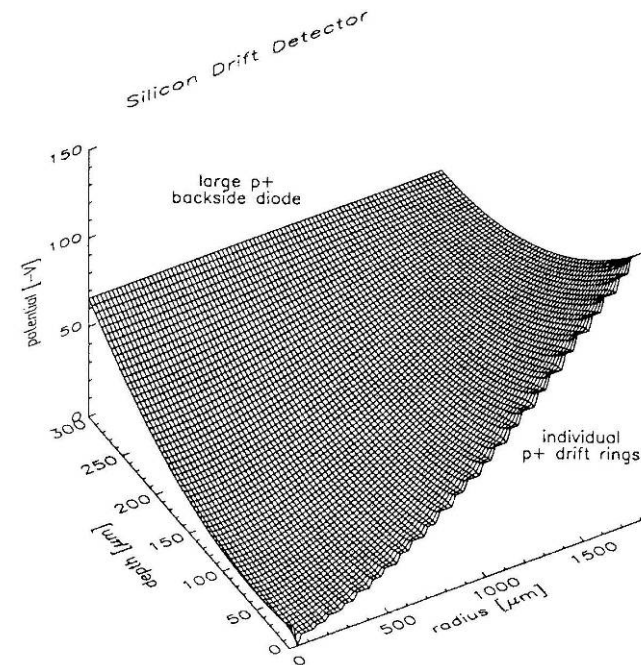


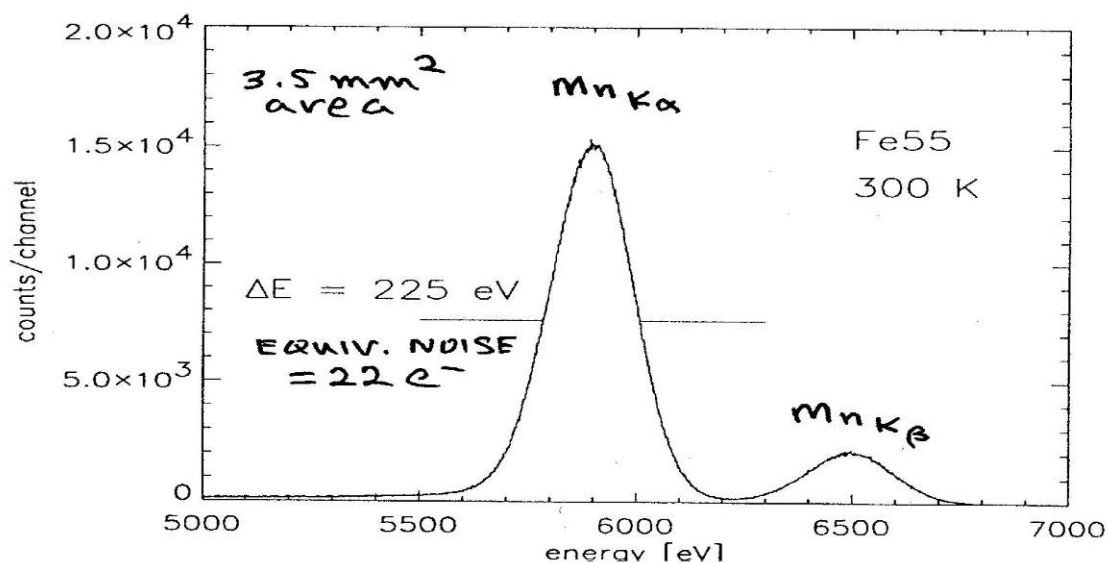
Fig. 2. Numerical simulation of the silicon drift detector. The simulated thickness of the detector is 300 μm , the simulated radius around the readout anode is 1800 μm comprising 23 p^+ field strips. Having a resistivity of 3 $\text{k}\Omega\text{cm}$ the maximum voltage for the devices with a diameter of 3.5 mm is about 150 V. The device's backside – the radiation entrance side – has a uniform p^+ implant resulting in the equipotential of less than 70 V.



Silicon Drift Detectors

These devices are known as silicon drift detectors. They have many advantages:

- The voltage divider and the input FET can be monolithically integrated into a single device.
- The collection electrode area is a small fraction of the total collection area, so the noise is low, even at room temperature.

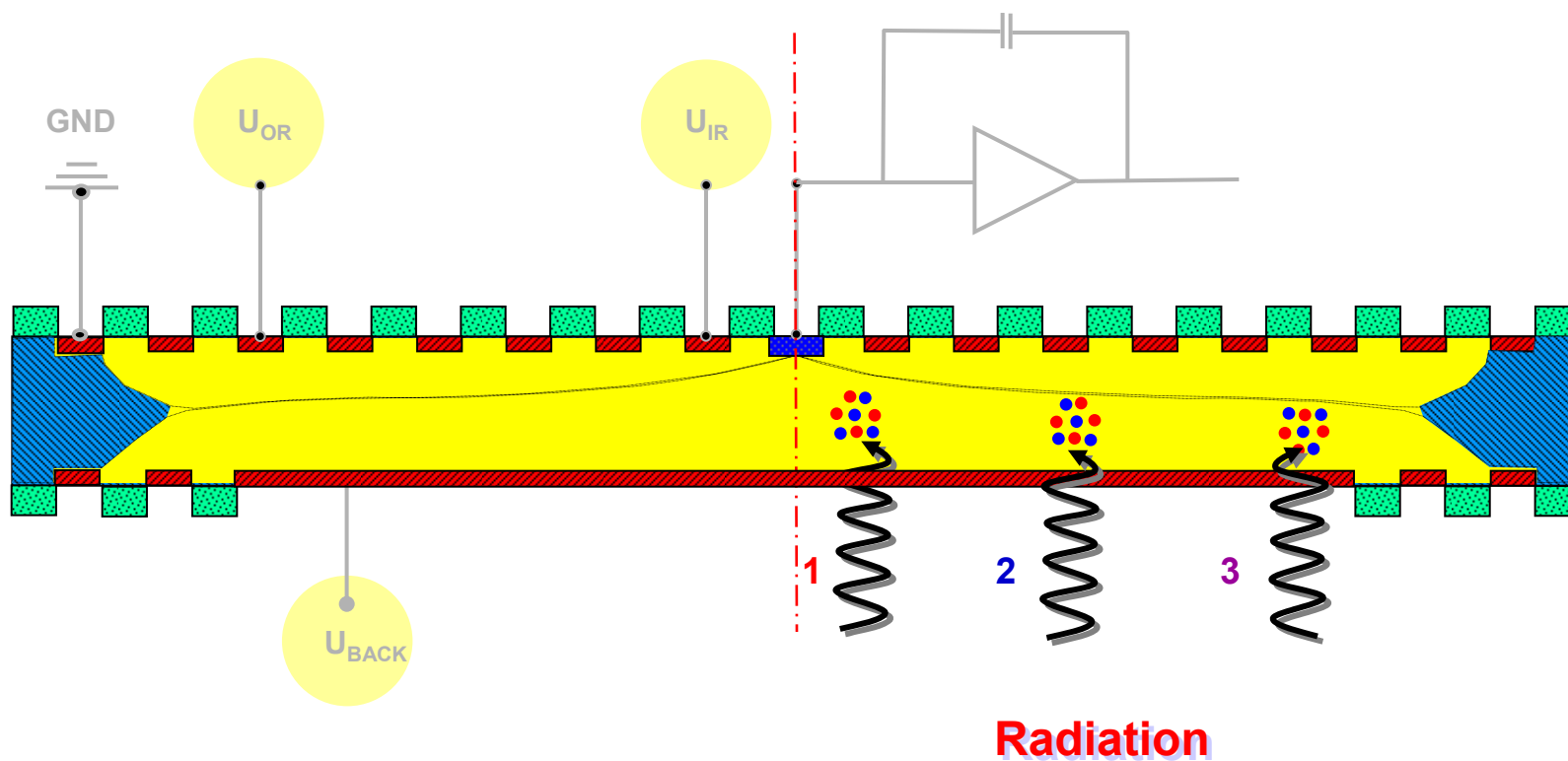


Lechner et al., *Nucl Instr Meth Phys Res A* 377 (1996) 346



Function of Silicon Drift Detector

(3)

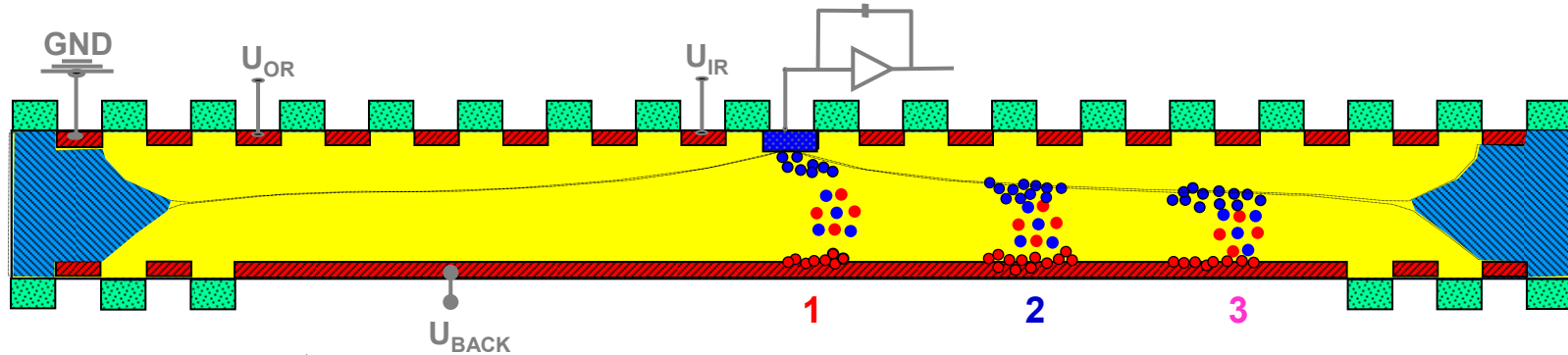


Absorption of x-rays

J. Kemmer, Andreas Pahlke CET04

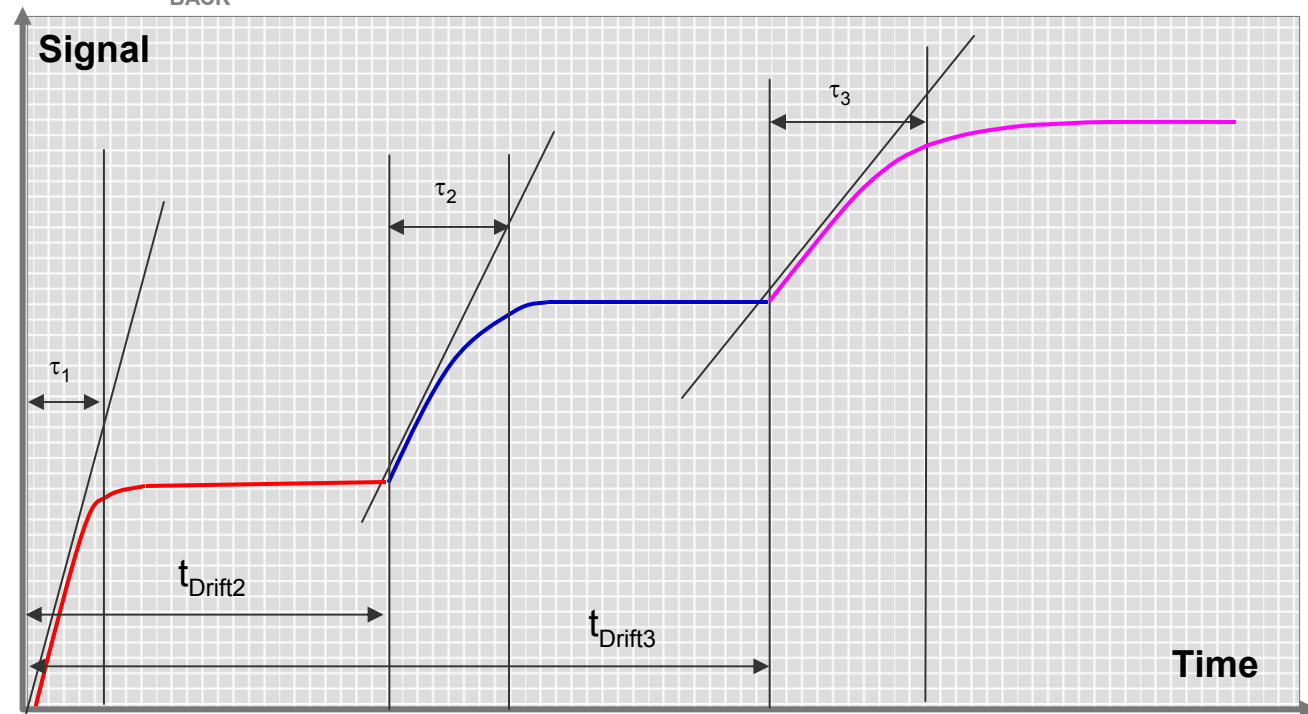


Function of Silicon Drift Detector (5)



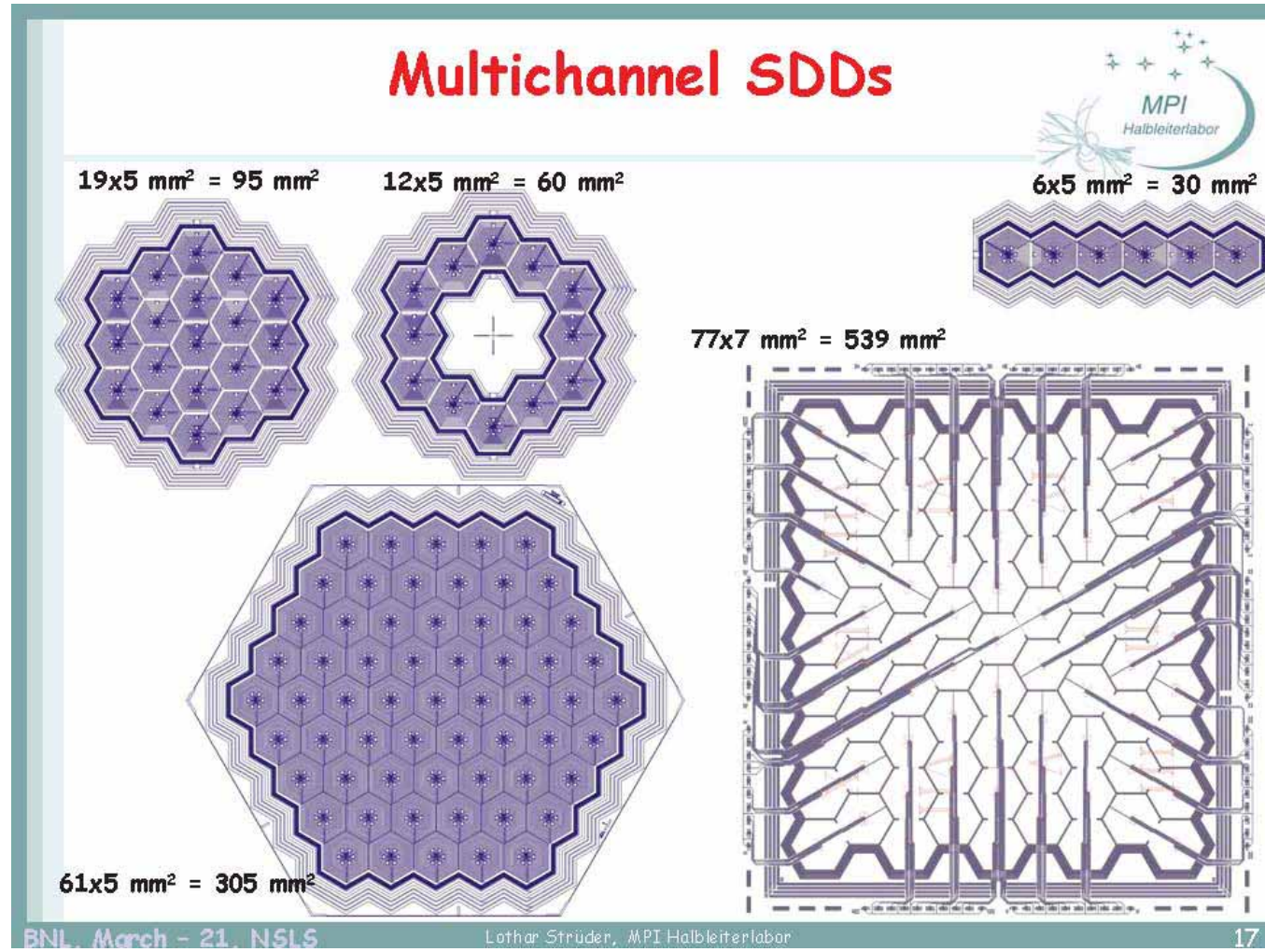
Charge Collection:

- Event 1 **signal 1**
- Event 2 **signal 2**
- Event 3 **signal 3**

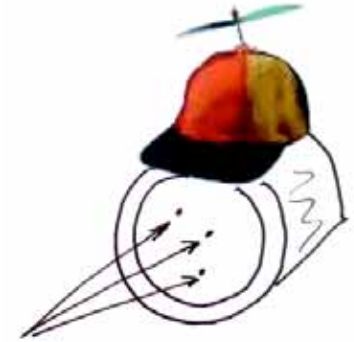


Silicon Drift Detectors

Silicon drift chambers can, in principle be made in a wide variety of shapes by placing smaller elements side-by-side. They have a promising future.



Current Imaging X-ray Detectors are “Simple”



Field is dominated by single snap-shot cameras with no built-in complex functionality.

- a) Film
- b) Image Plates
- c) CCDs, either directly or phosphor-coupled, dominate SR

Drawbacks:

- Have to stop experiment after each image.
- Data function processing is done off-line.



Integrated Circuit technology now make “Intelligent” Detectors Feasible

An intelligent Pixel Array
Detectors (PAD) has
sophisticated data processing
functions built into each pixel of
the detector.



Basic Pixel Array Detector (PAD)

Diode Detection Layer

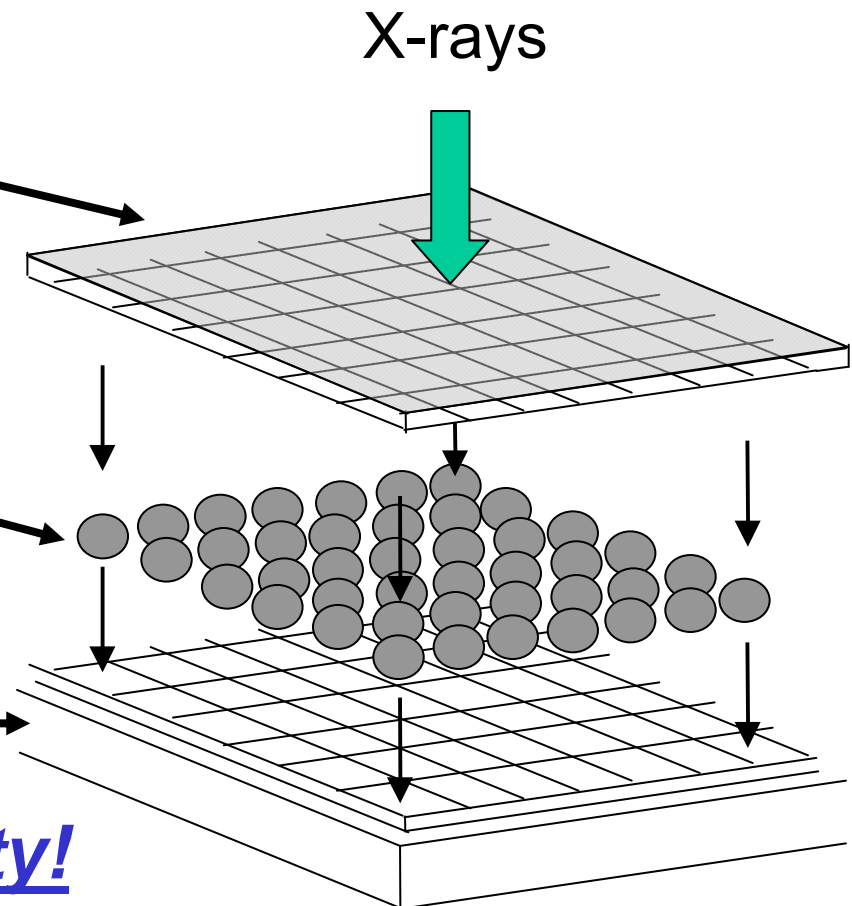
- Fully depleted, high resistivity
- Direct x-ray conversion in Si

Connecting Bumps

- Solder, 1 per pixel

CMOS Layer

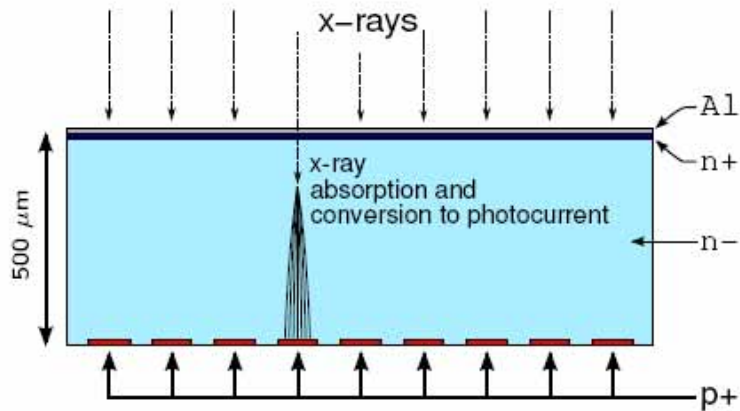
- Signal processing
- Signal storage & output



Gives enormous flexibility!



Diode Layer



Diode Cross Section

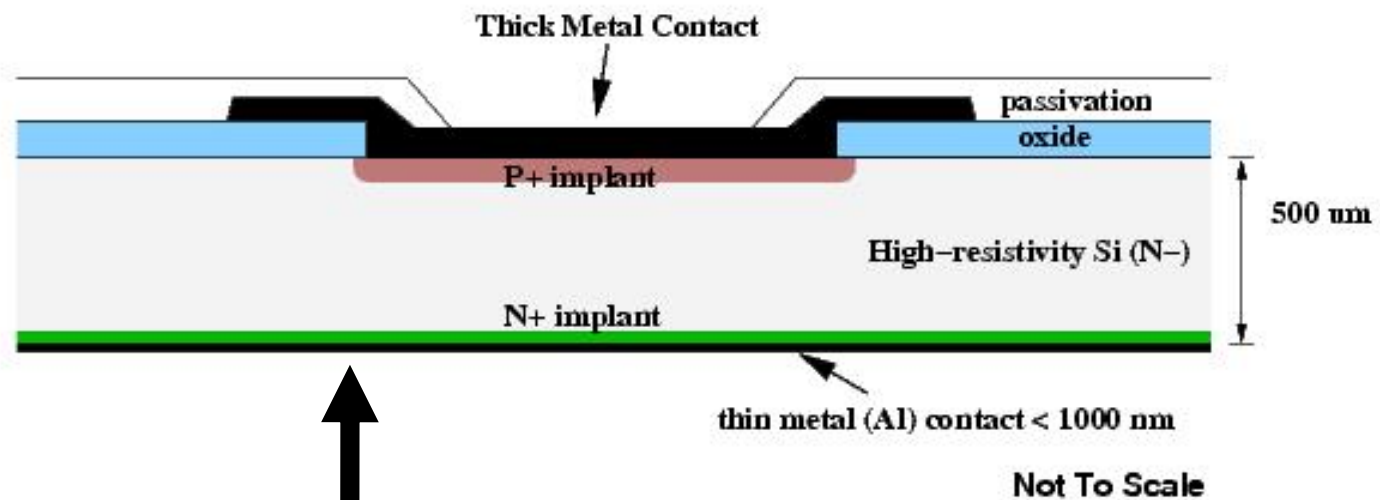
- Photodiode layer → high resistivity silicon (3,000–10,000 ohm-cm).
- Thick detector → effective up to 20 keV x-rays.

Benefits of Direct Detection

- High Efficiency and Low Noise Contribution
 - Mixed-Mode PAD
 - 2740 ± 20 carriers per 10 keV x-ray.
 - Phosphor Coupled CCD
 - 10 to 30 ± 10 to 20 electrons per 10 keV x-ray.
- Sub-Pixel Point Spread



Diode Structure (Single Pixel Connection)

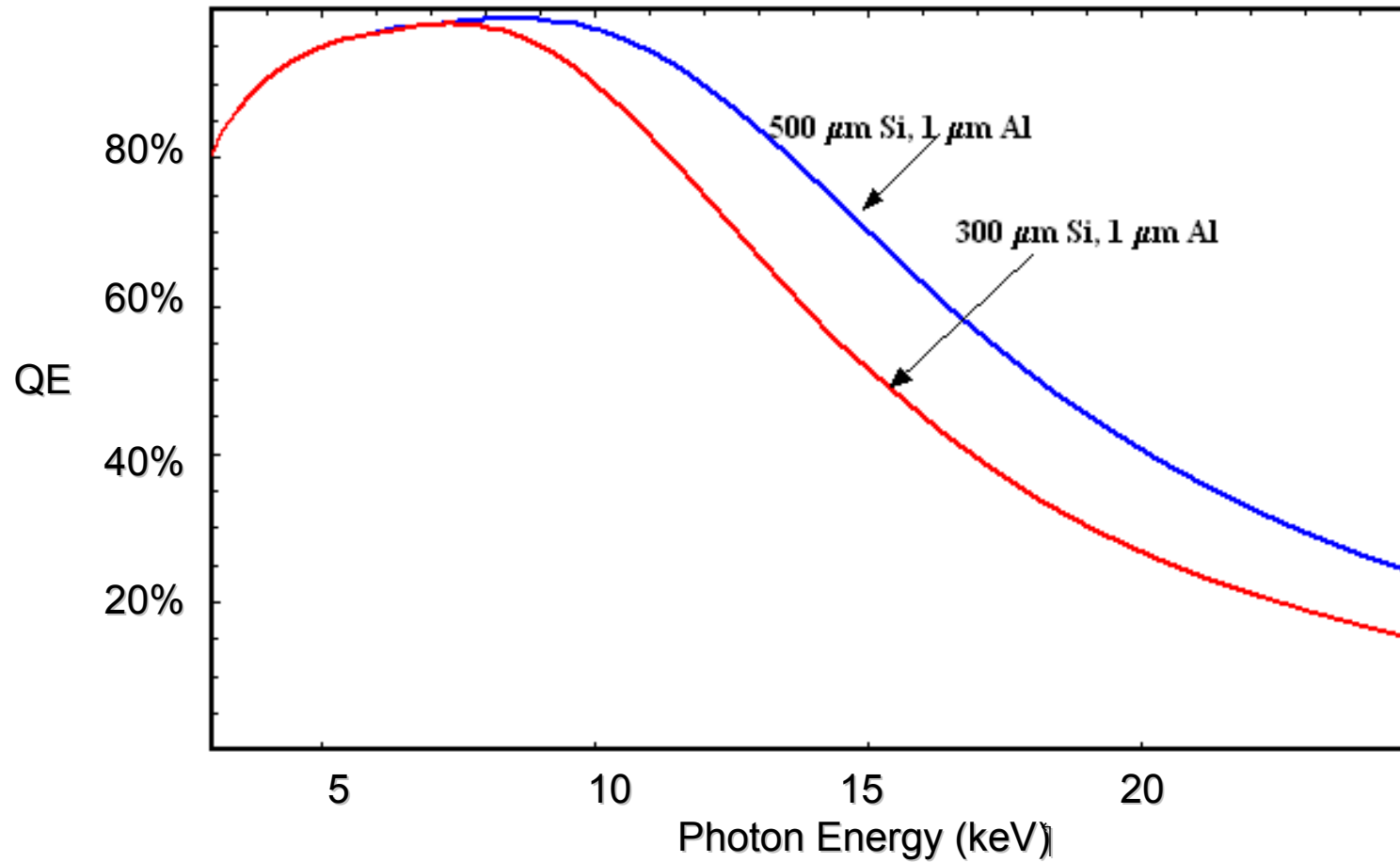


x-rays

Direct conversion of x-rays to charge carriers in silicon. Approx. 1 charge carrier pair/ 3.64 eV, or 2200 electrons/ absorbed 8 keV x-ray.



Diode Efficiency



PADs come in two varieties

Photon counting PADs (Europe).

- Front ends count each x-ray individually. (PILATUS, Medipix)
- Serious drawback for high-speed imaging: Count-rate limited by electronics to $\sim 10^6$ - 10^7 x-rays/pix/sec.



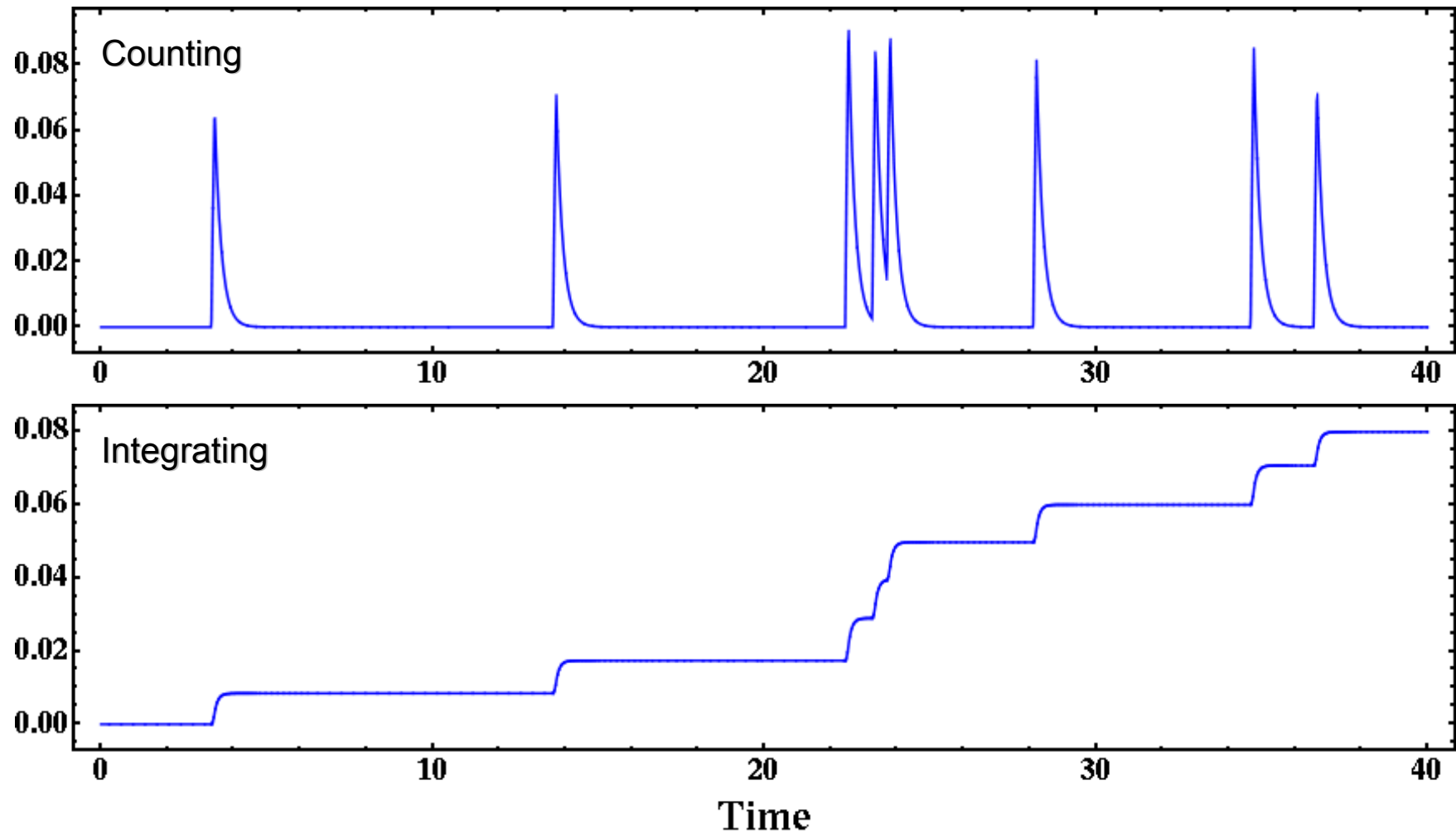
SLS
PILATUS

Integrating PADs (Cornell).

- Use an integrating front-end to avoid the count-rate bottleneck.
- Capable of handling enormous count-rate.
- The “intelligence” is determined by the CMOS electronics.
- Existing variants include LCLS, ADSC
- Proposed variants include:
 - Submicrosecond successive framing imager
 - PAD with time autocorrelator assigned to each pixel

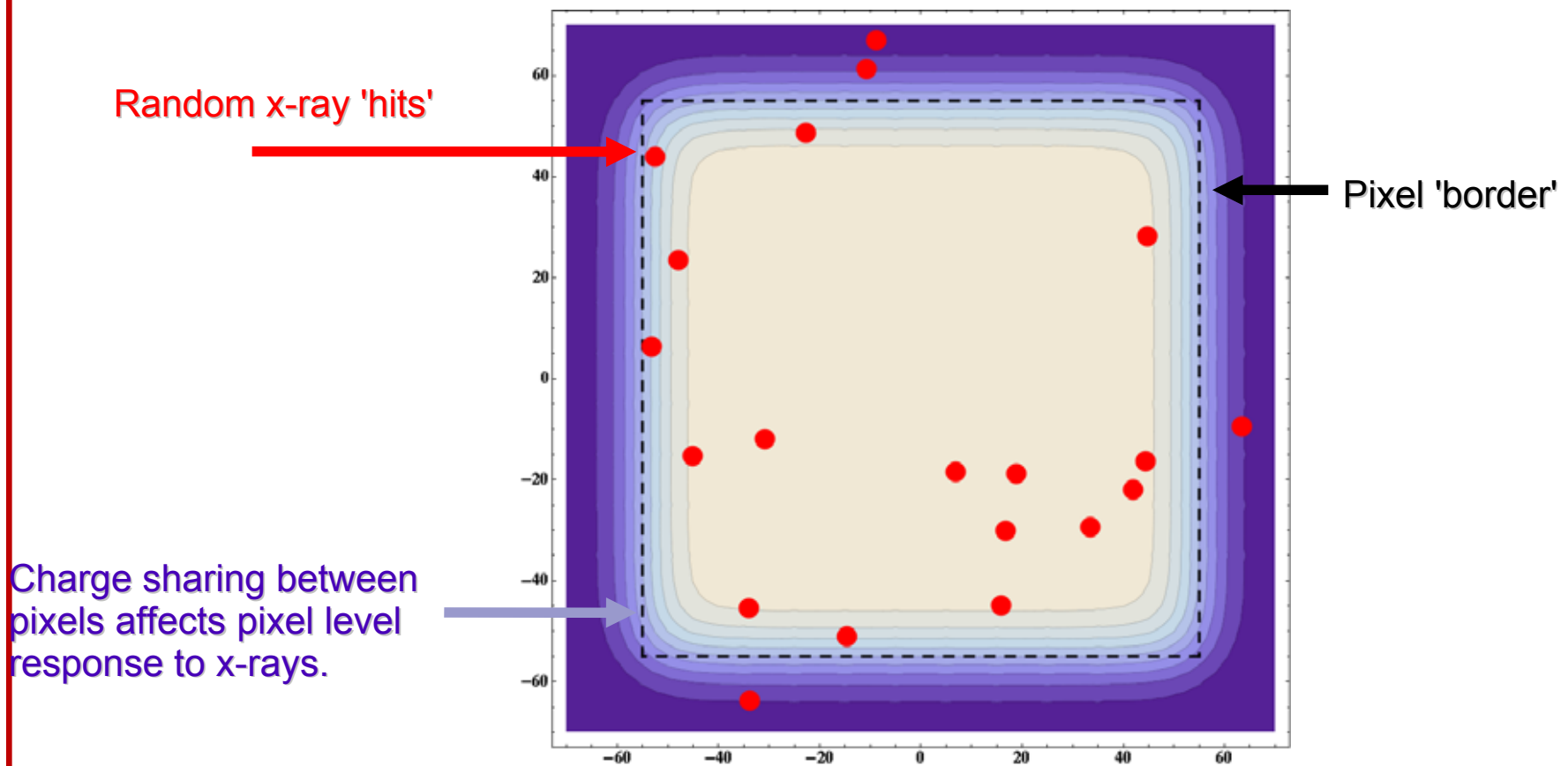


Pixel-Level Counting vs. Integration

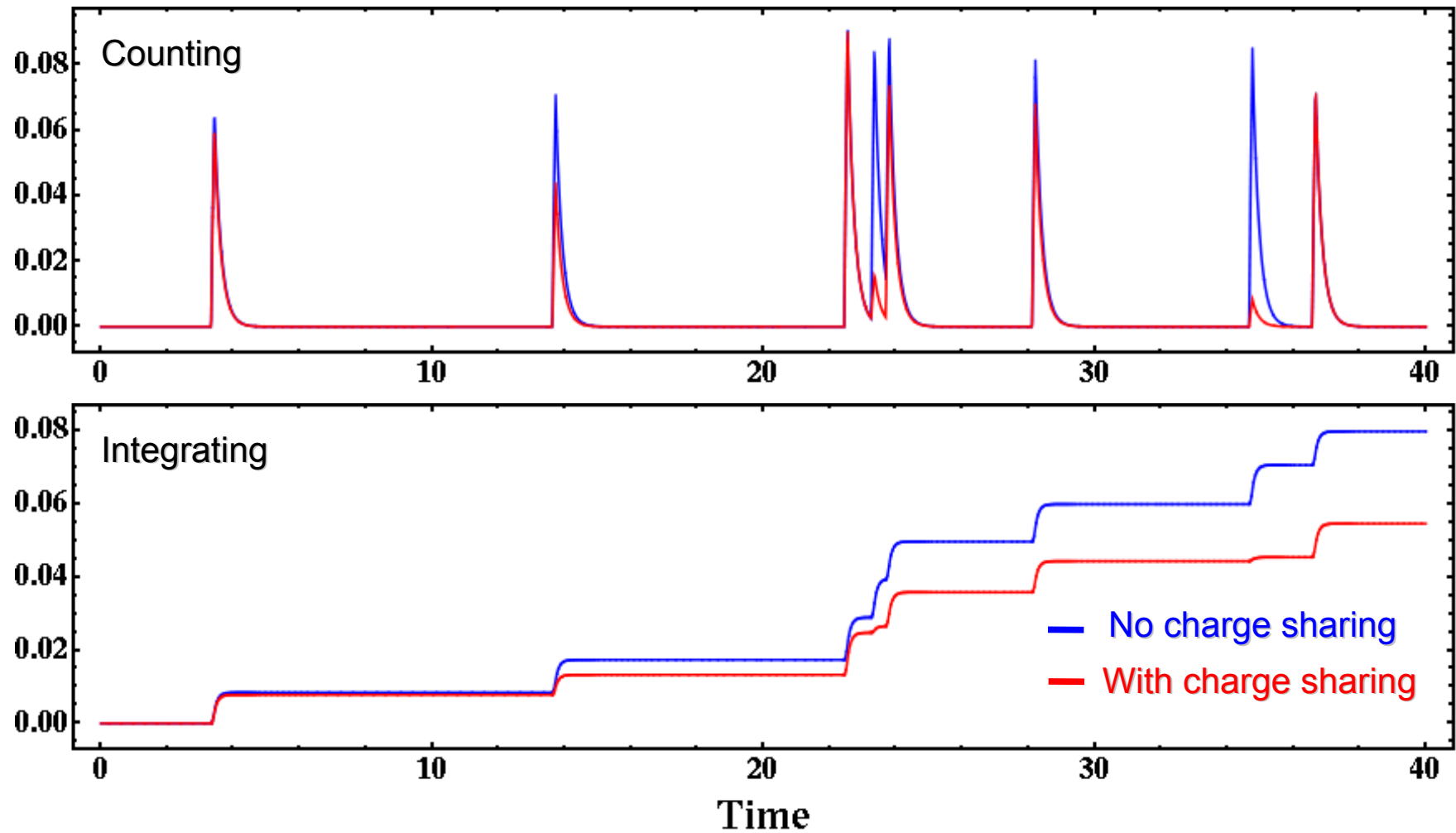


Pixel-Level Counting vs. Integration

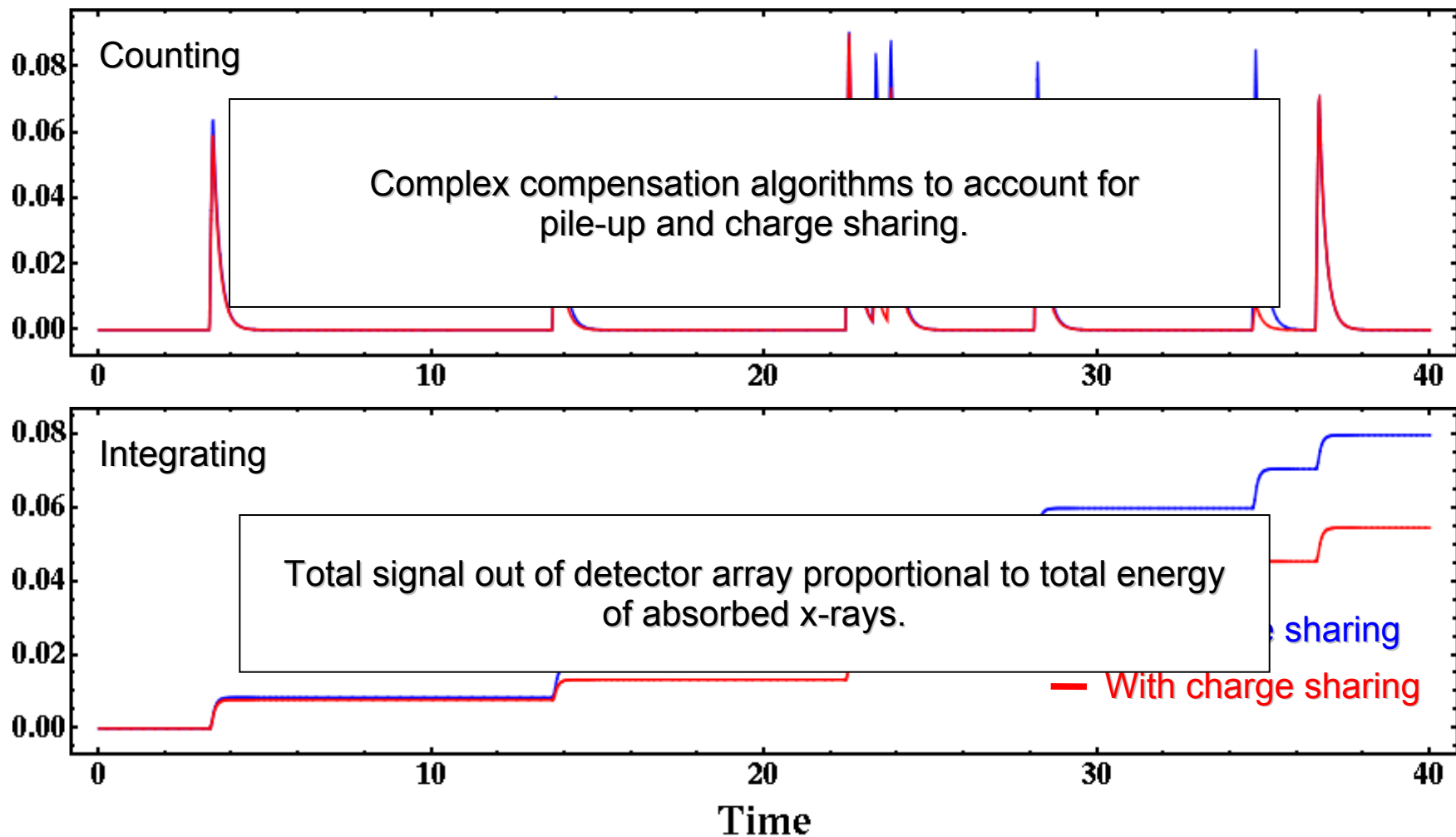
- **Signal also spatial function.**



Pixel-Level Counting vs. Integration



Pixel-Level Counting vs. Integration



Example 1: High Speed Imaging

Requirements: Rapid Framing Imager

In pix storage for 8 frames

Selectable integration time (μs to seconds)

Dead time $<$ few μs

Well-depth $> 10^4$ x-rays/pixel/frame (for 1% statistics)

Count rate $> 10^{10}$ x-rays/pixel/s  Analog integration needed

Standard CMOS fabrication service



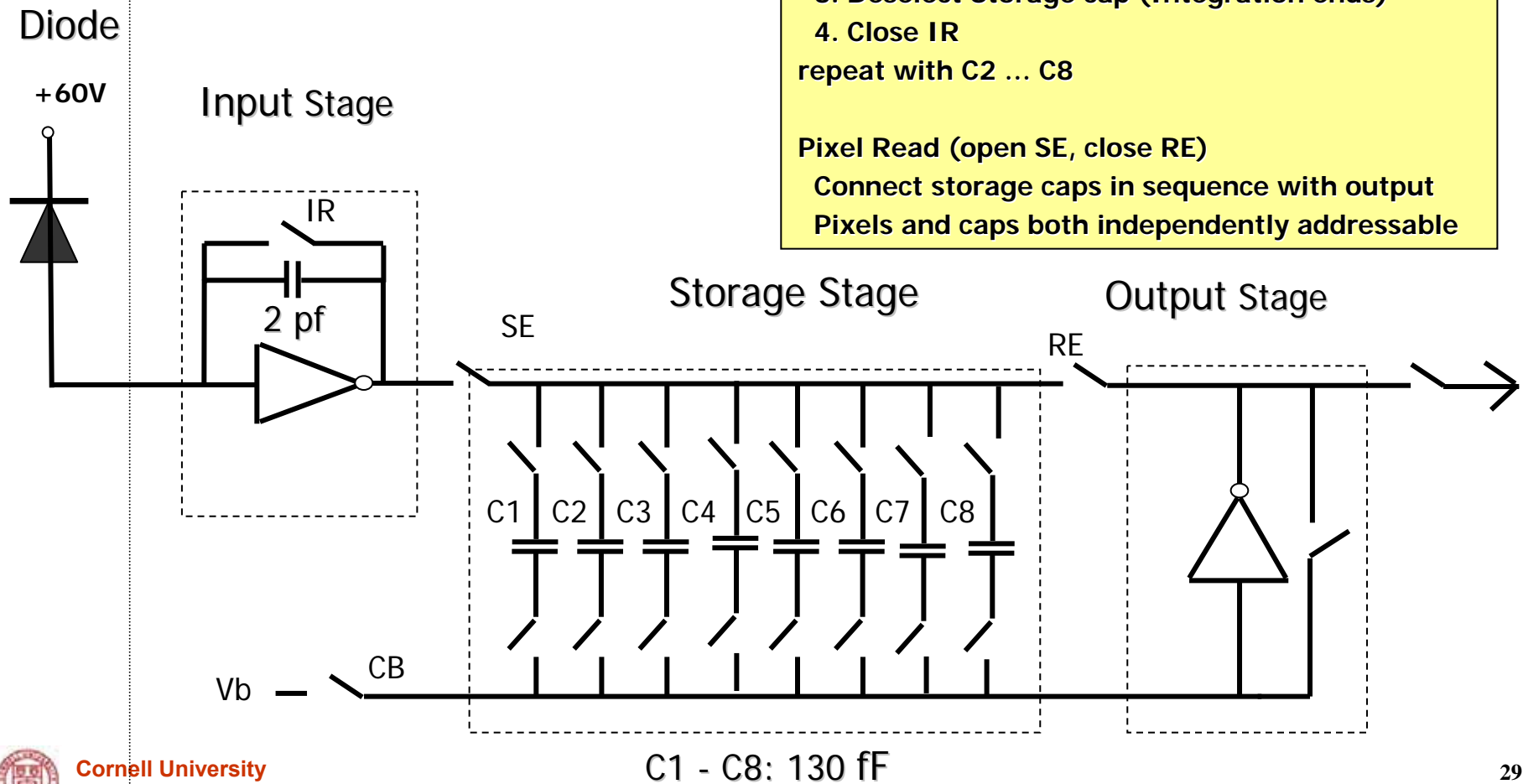
Application Examples

- **High-flux radiography**
 - **Liquid jets**
 - **Shock waves**
 - **Crack propagation**
 - **Protein structure determination w/out crystals**
 - **Phase transitions in alloys, polymers & Liq. Crystals**
 - **Materials failure due to fatigue**
 - **Cavitation**
 - **Enzyme activation & function**
 - **Etc.**



Cornell Prototype Integrating PAD

Rossi et al, *J. Synchr Rad*, 6 (1999) 1096.



High speed radiography

Supersonic spray from diesel fuel injector

X-ray beam

- **CHESS Beamline D-1**
- **6 keV (1% bandpass)**
- **2.5 mm x 13.5 mm (step sample to tile large area)**
- **$10^8 - 10^9$ x-rays/pix/s**
- **$5.13 \mu\text{s}$ integration (2x ring period)**

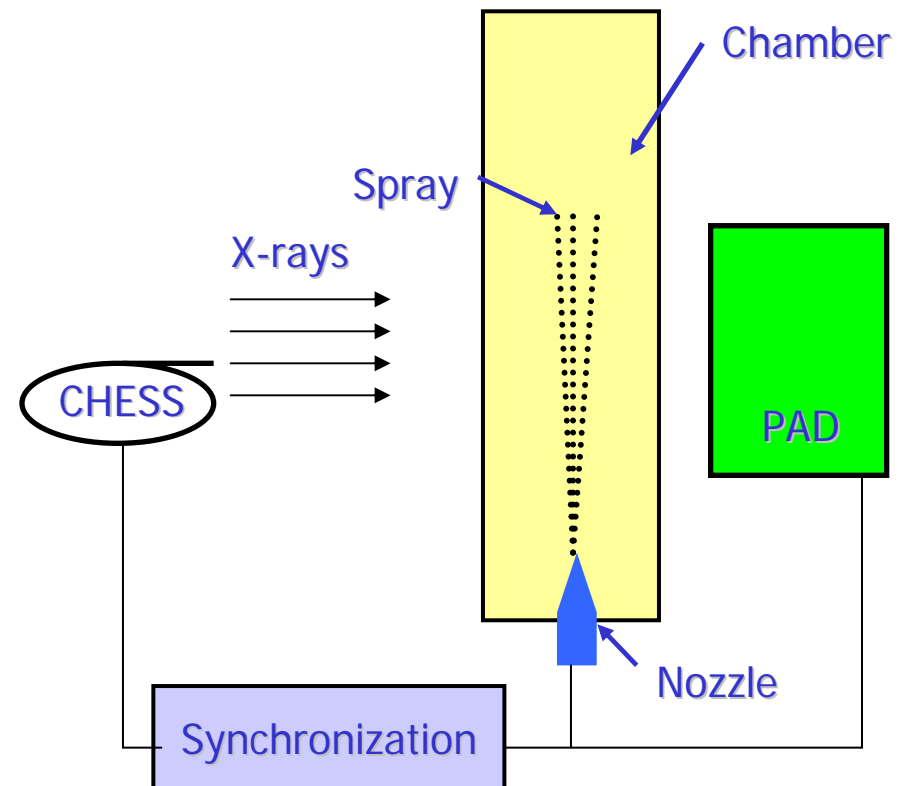
Diesel Fuel Injection System

- **Cerium added for x-ray contrast**
- **1350 PSI gas driven**
- **1.1 ms pulse**
- **1 ATM SF_6 in chamber**

Collaboration: Jin Wang (APS) & S.M. Gruner (Cornell)

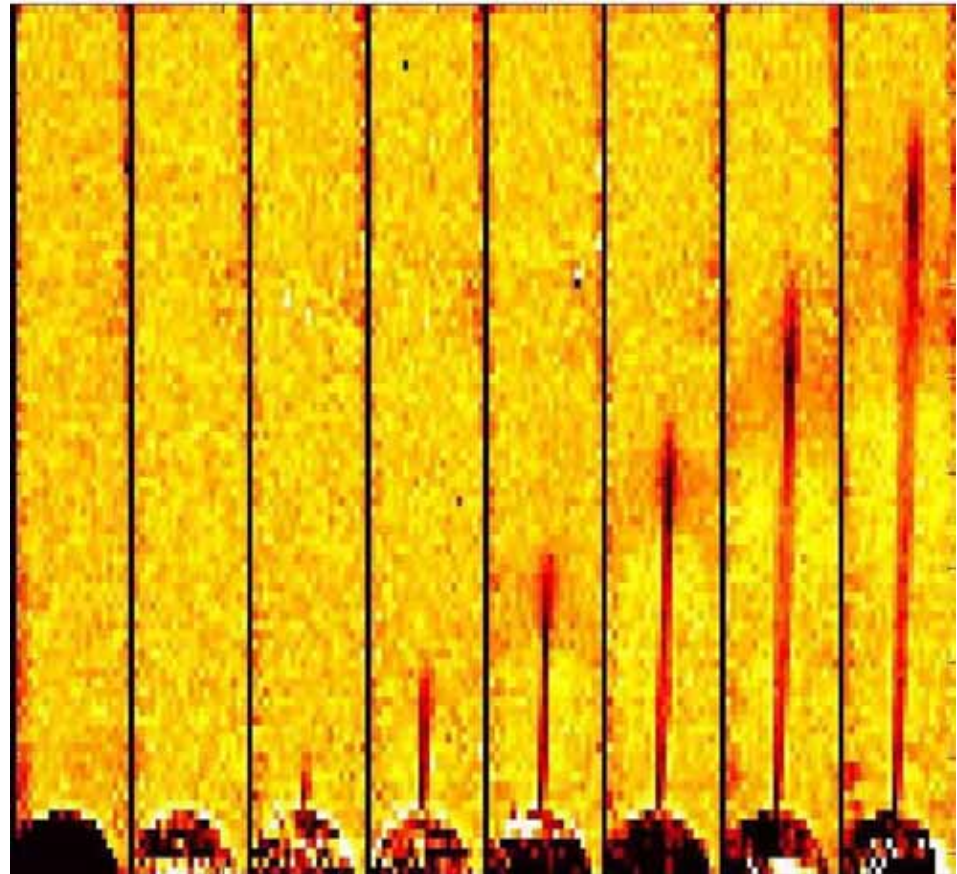
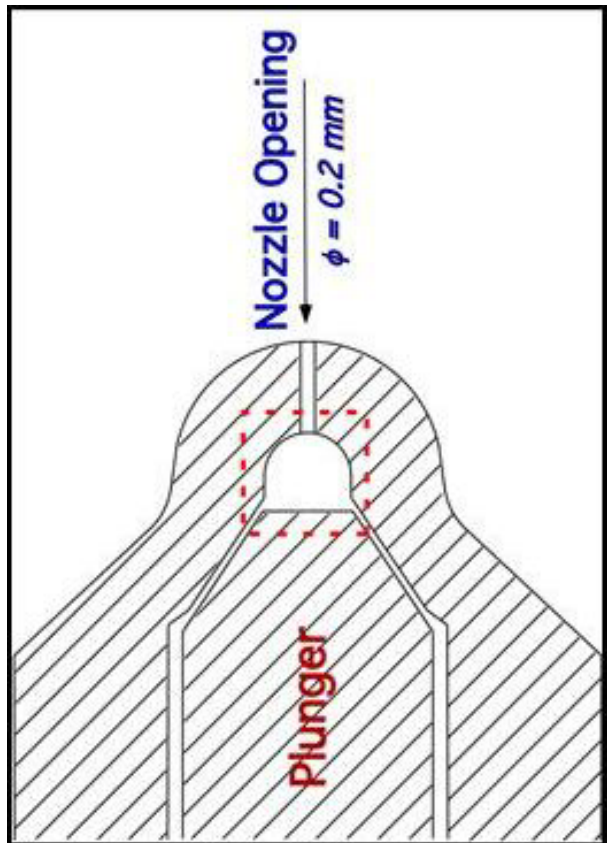
See: McPhee, Tate, Powell, Yue, Renzi, Ercan, Narayanan, Fontes, Walther, Schaller, Gruner & Wang

***Science* 295 (2002) 1261-1263.**



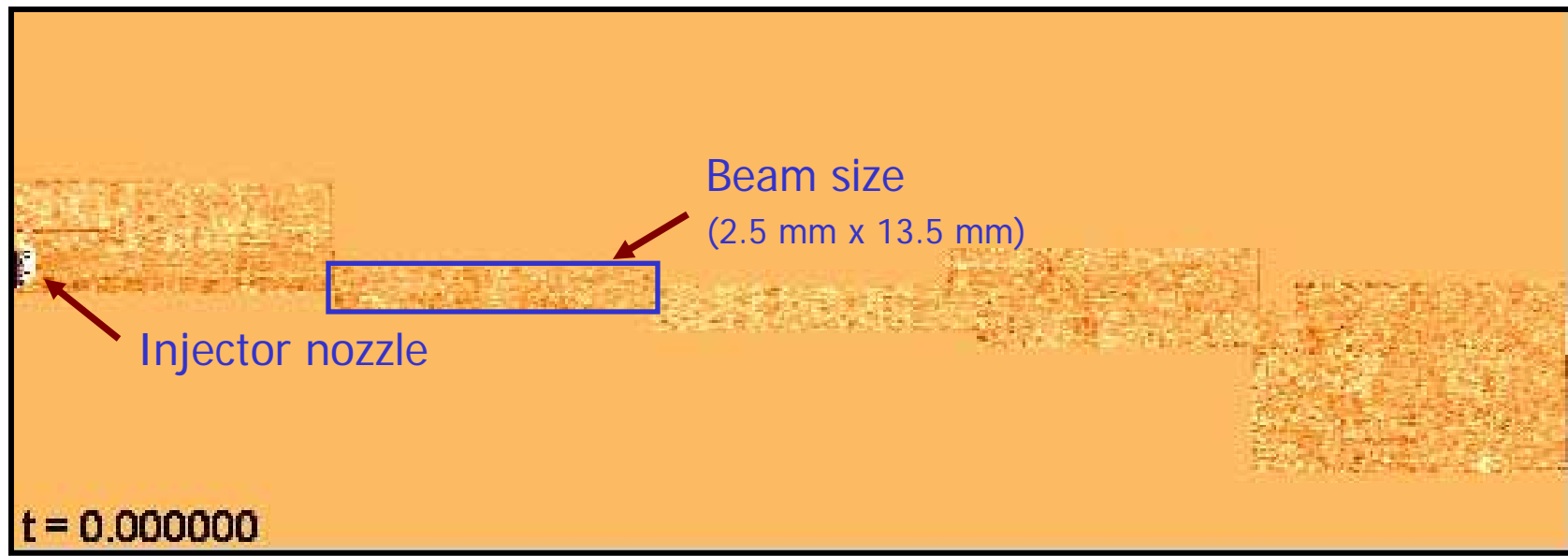
High speed radiography

Supersonic spray from diesel fuel injector



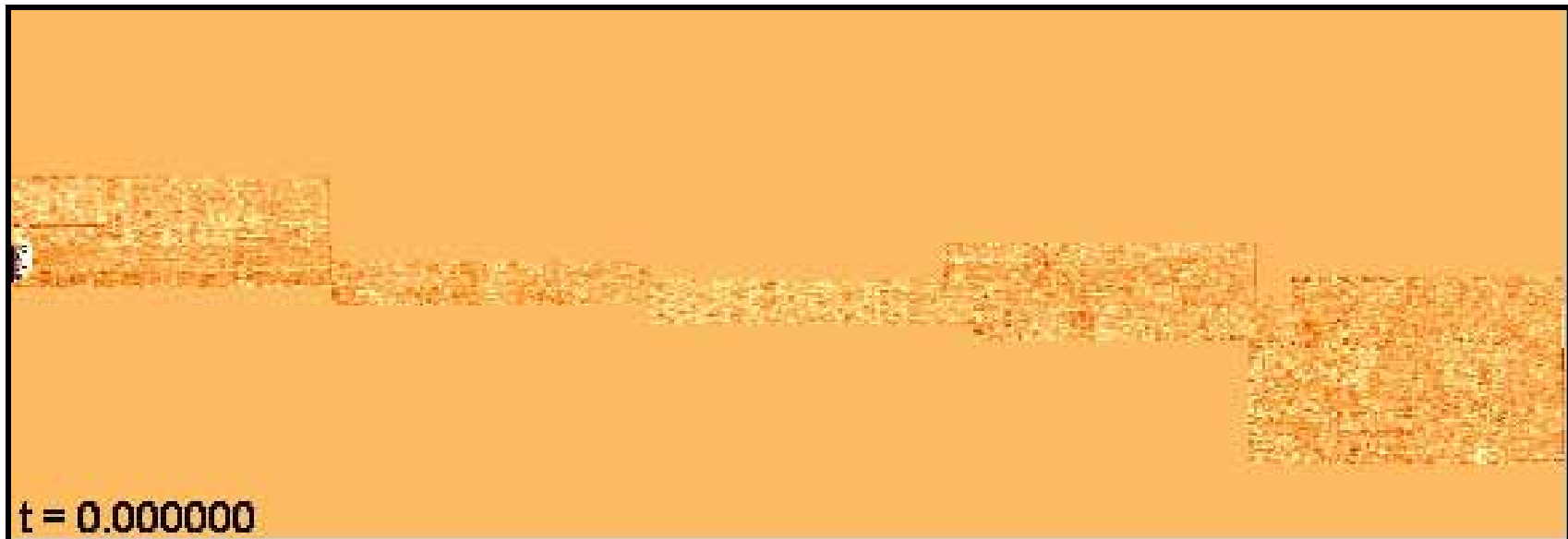
Diesel fuel injector spray

- 1.3 ms time sequence (composite of 34 sample positions)
- 5.13 μs exposure time (2.56 μs between frames)
- 168 frames in time (21 groups of 8 frames) Average 20x for S/N
- Sequence comprised of 5×10^4 images

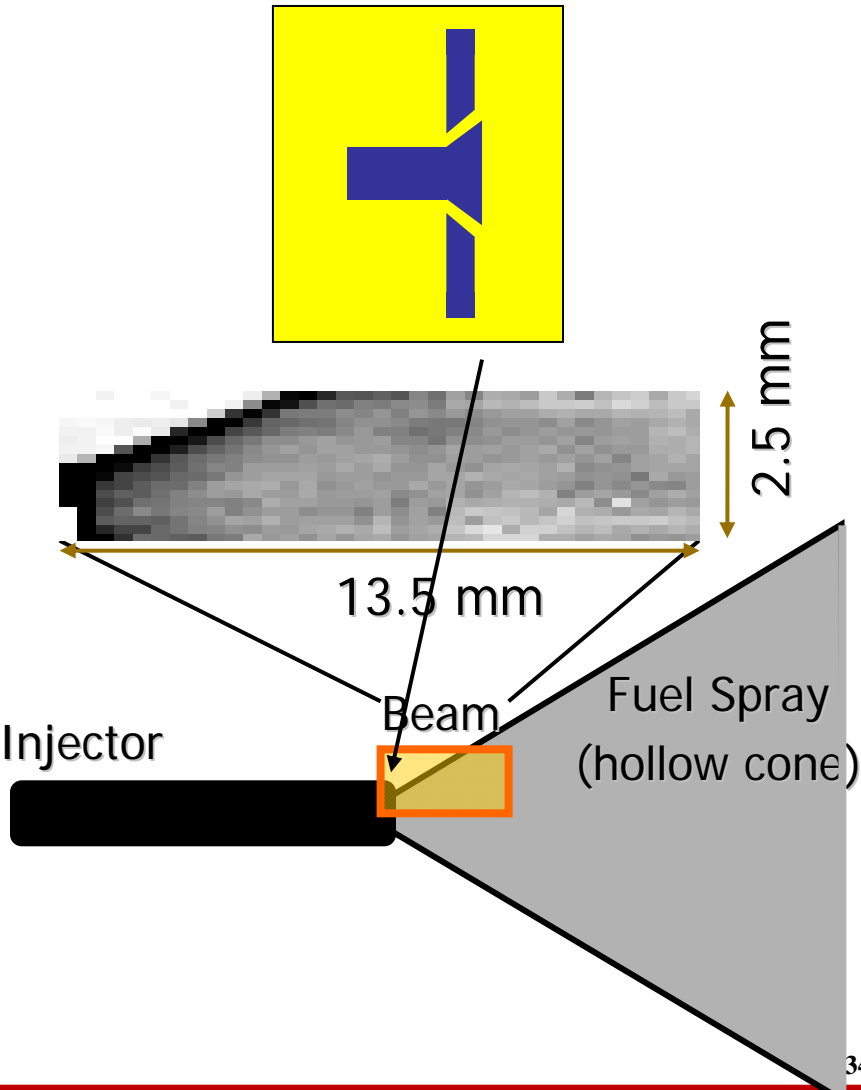
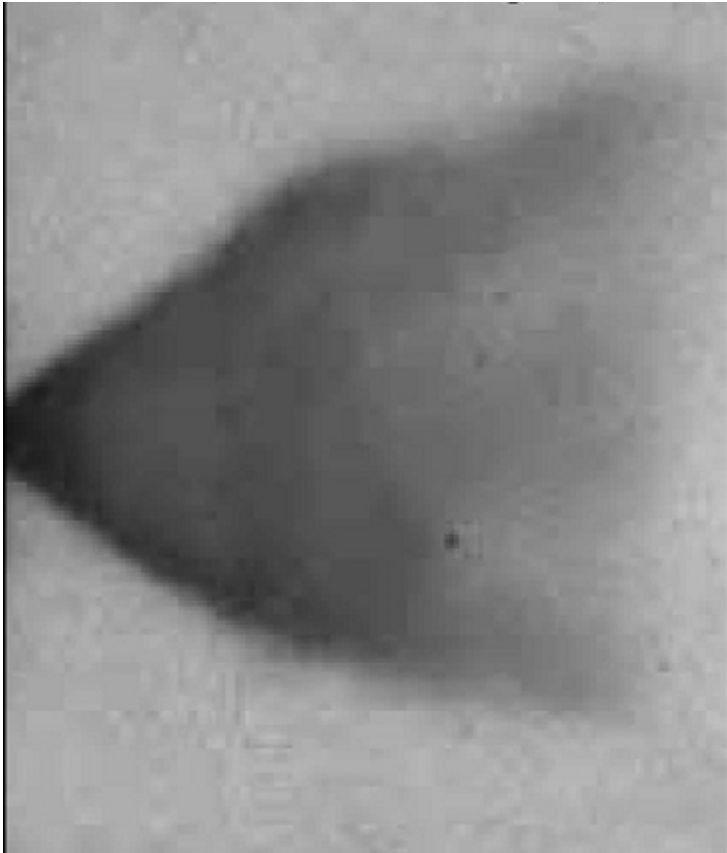


Diesel fuel injector spray

- 1.3 ms time sequence (composite of 34 sample positions)
- 5.13 μs exposure time (2.56 μs between frames)
- 168 frames in time (21 groups of 8 frames) Average 20x for S/N
- Sequence comprised of 5×10^4 images



Gasoline fuel injector spray



Gasoline fuel injector spray

X-ray beam

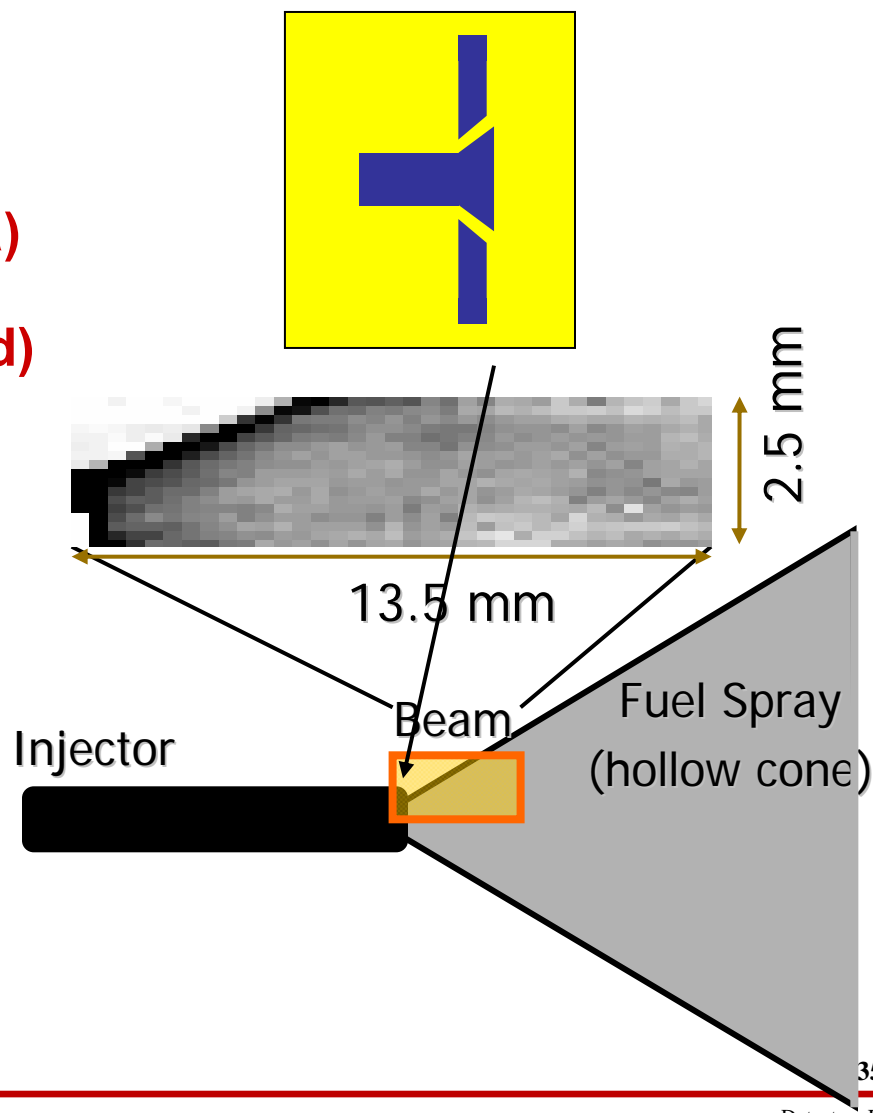
- **CHES Beamline D-1**
- **6 keV (1% bandpass)**
- **2.5 mm x 13.5 mm**
- **(step sample to tile large area)**
- **10^9 x-rays/pix/s**
- **5.13 μ s integration (2x ring period)**

Fuel injection system

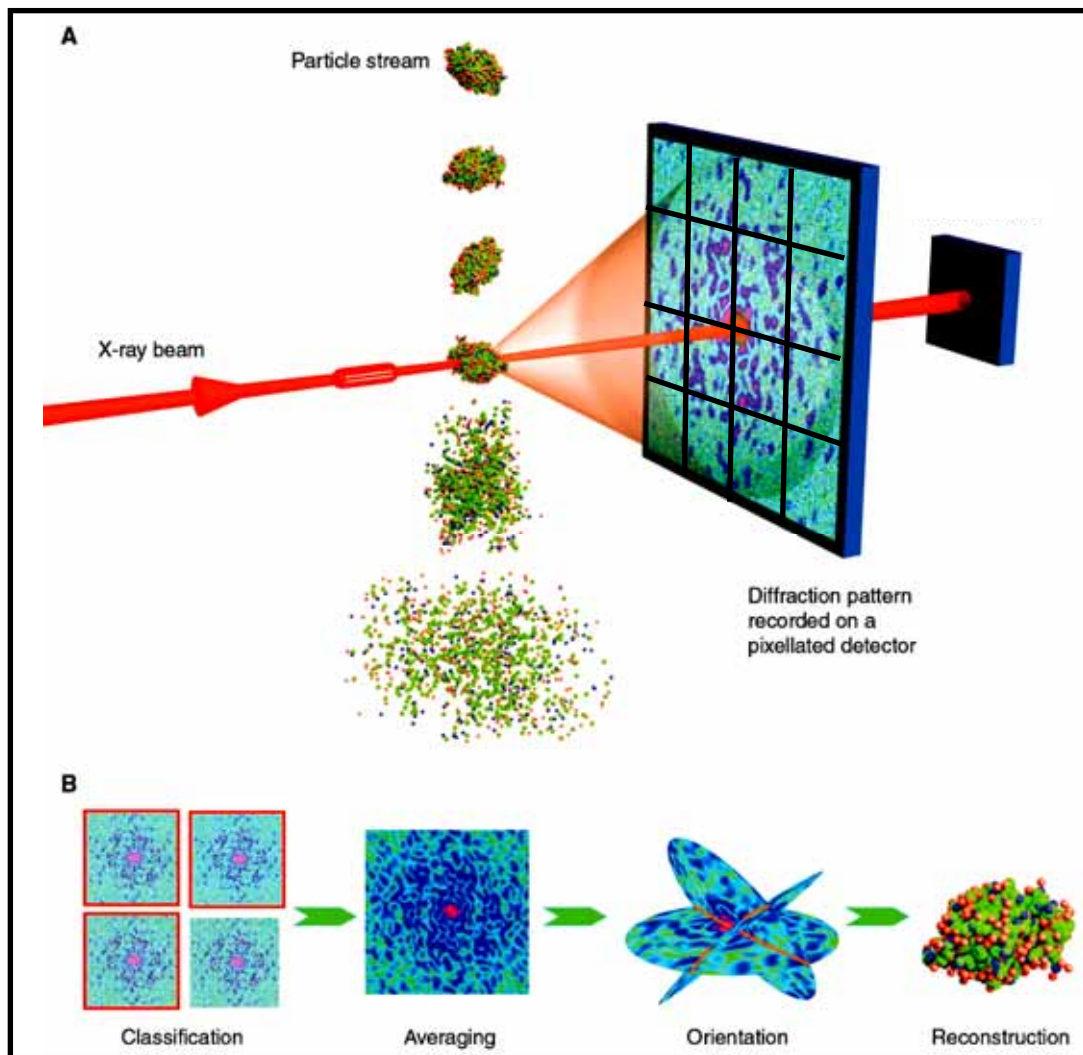
- **Cerium added for x-ray contrast**
- **1000 PSI gas driven**
- **1 ms pulse**
- **1 ATM Nitrogen**

Collaboration: Jin Wang (APS) & S.M. Gruner (Cornell)

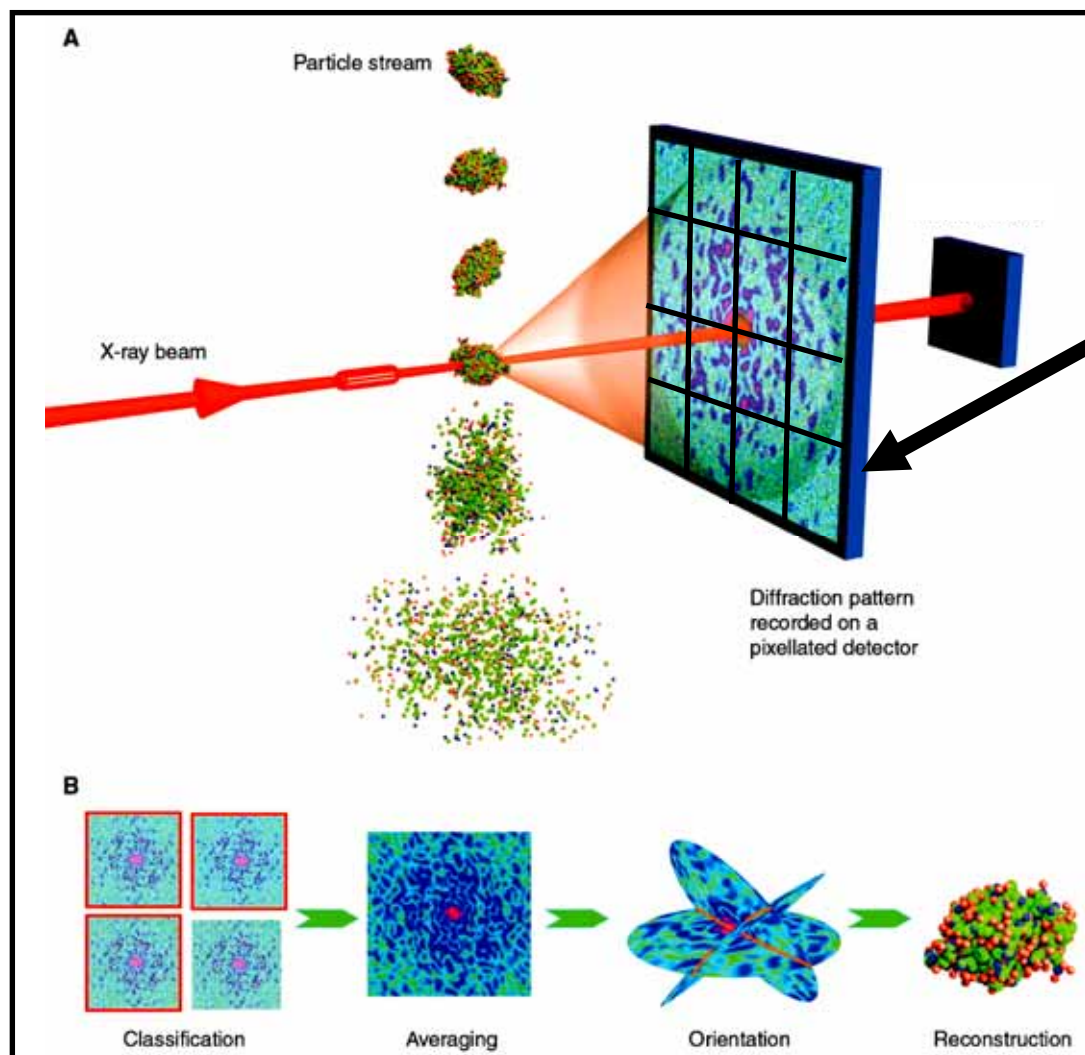
**See: Cai, Powell, Yue, Narayanan, Wang, Tate, Renzi, Ercan, Fontes & Gruner
Appl. Phys. Lett. 83 (2003) 1671.**



Example 2: LCLC Coherent Imaging Experiment



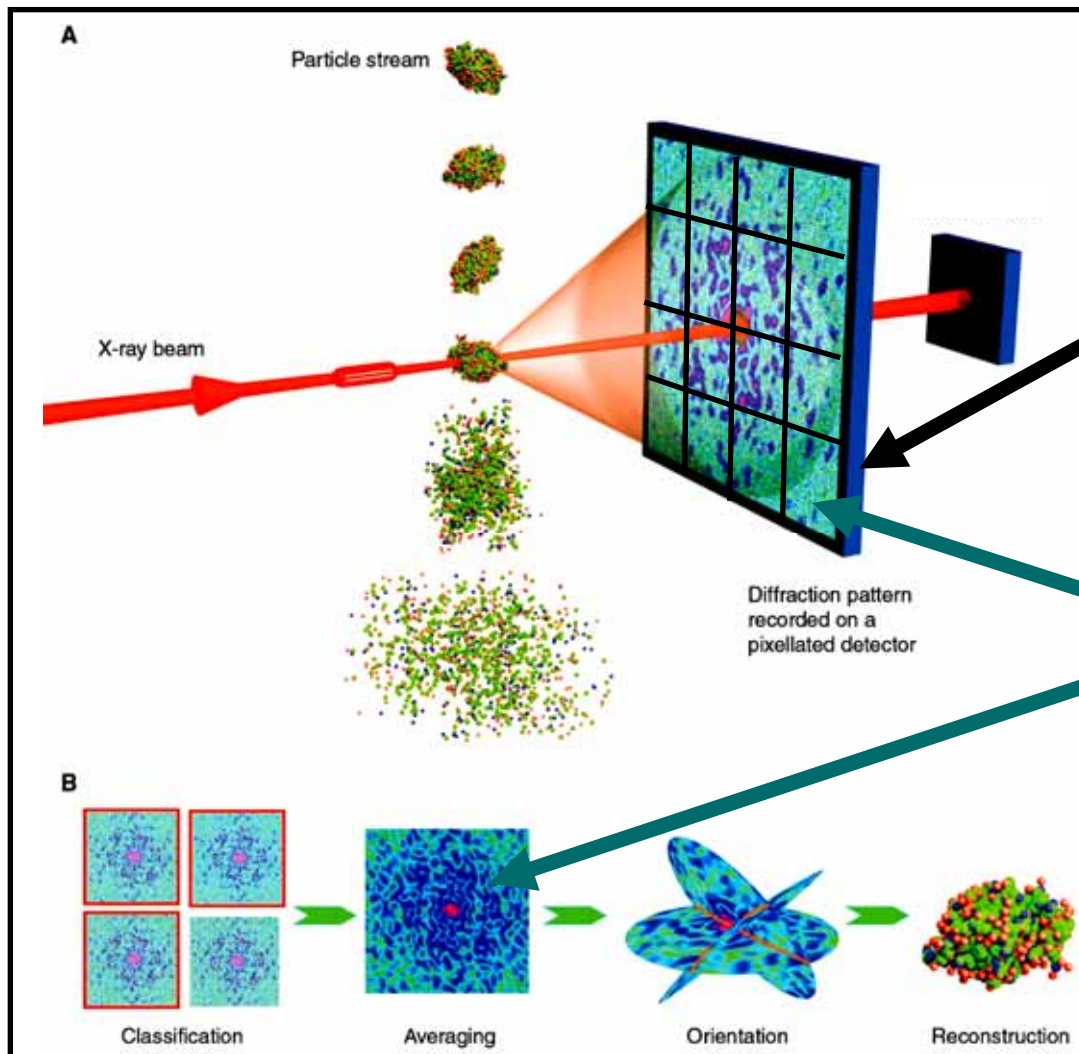
Example 2: LCLC Coherent Imaging Experiment



- Tiled PAD.
- 120 Hz frame.



Example 2: LCLC Coherent Imaging Experiment



- Tiled PAD.
- 120 Hz frame.

- Diffuse Scattering
- Variable envelope



Requirements

Parameter	Minimum Requirement
Energy Range	4-8 keV
Well-depth/pixel	10^3
Readout Frame rate	120Hz
Signal/Noise	>3 for single 8 keV photon
DQE	> 90% at 8 keV
Pixel size	100-200μm
Detector Area	500x500 pixels

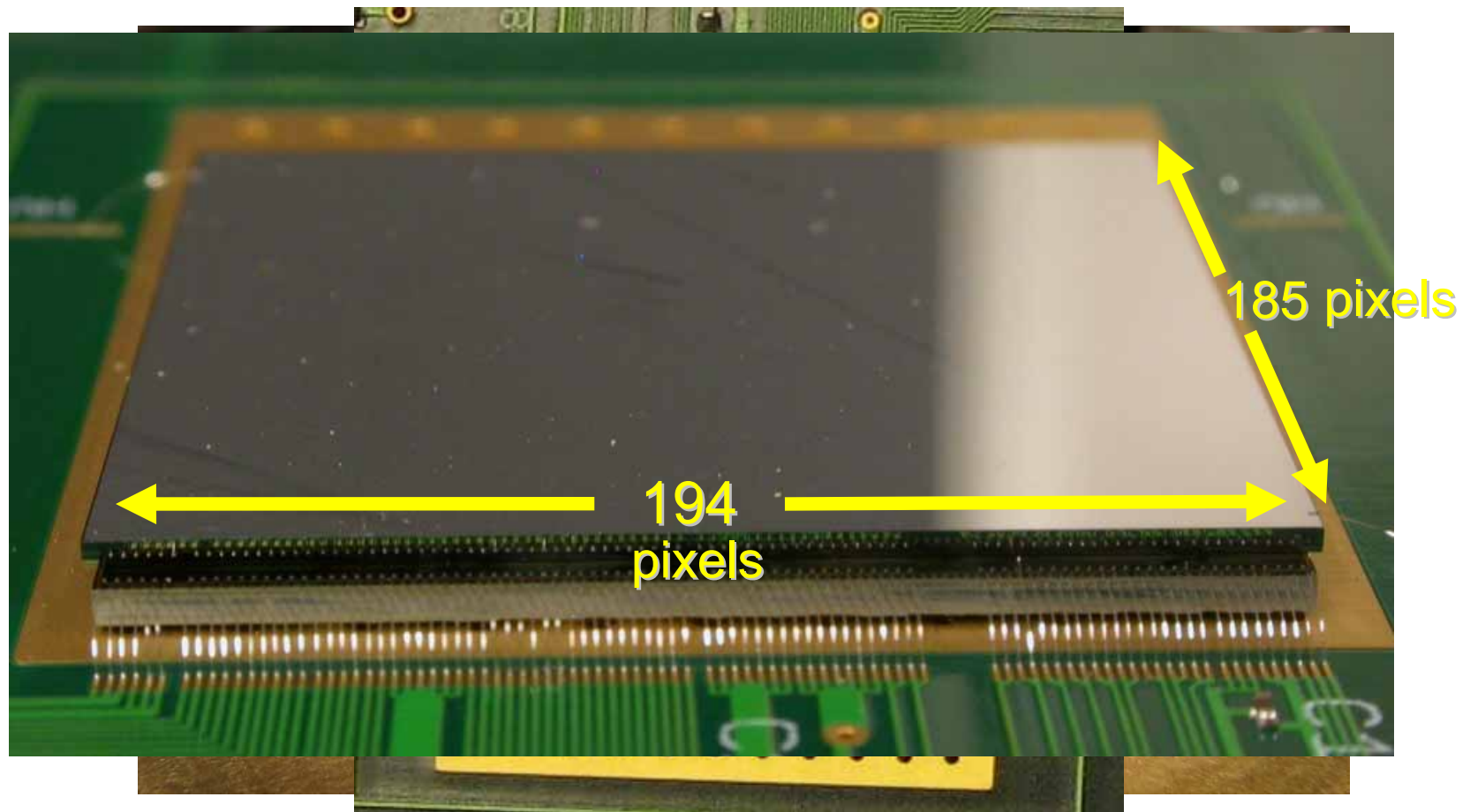


Requirements

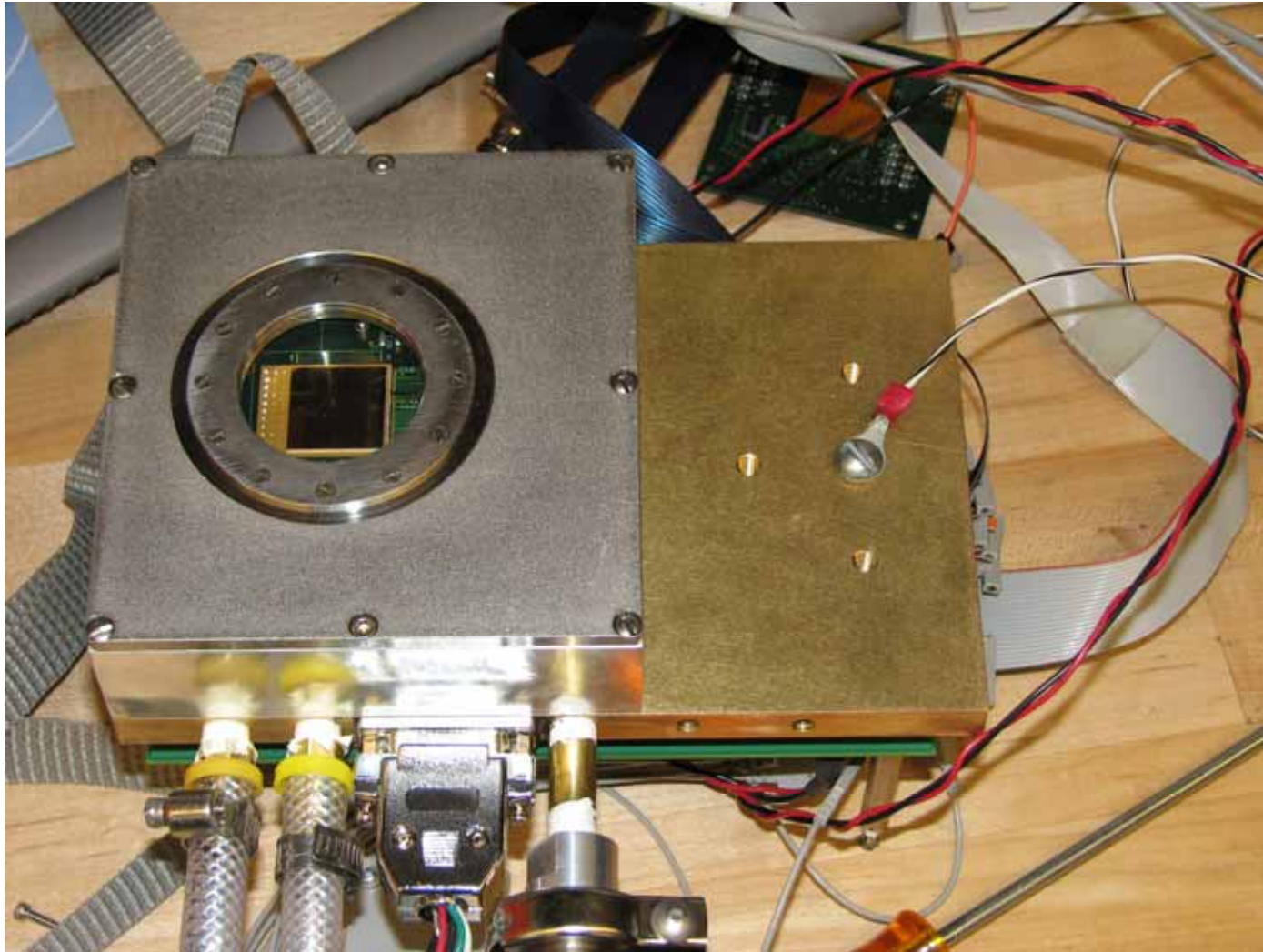
Parameter	Minimum Requirement
Energy Range	4-8 keV
Well-depth/pixel	10^3  > 2500 8 keV x-rays/pixels/image
Readout Frame rate	120Hz
Signal/Noise	>3 for single 8 keV photon
DQE	> 90% at 8 keV
Pixel size	100-200 μ m  110 x 110 microns
Detector Area	500x500 pixels  1516 x 1516 pixels



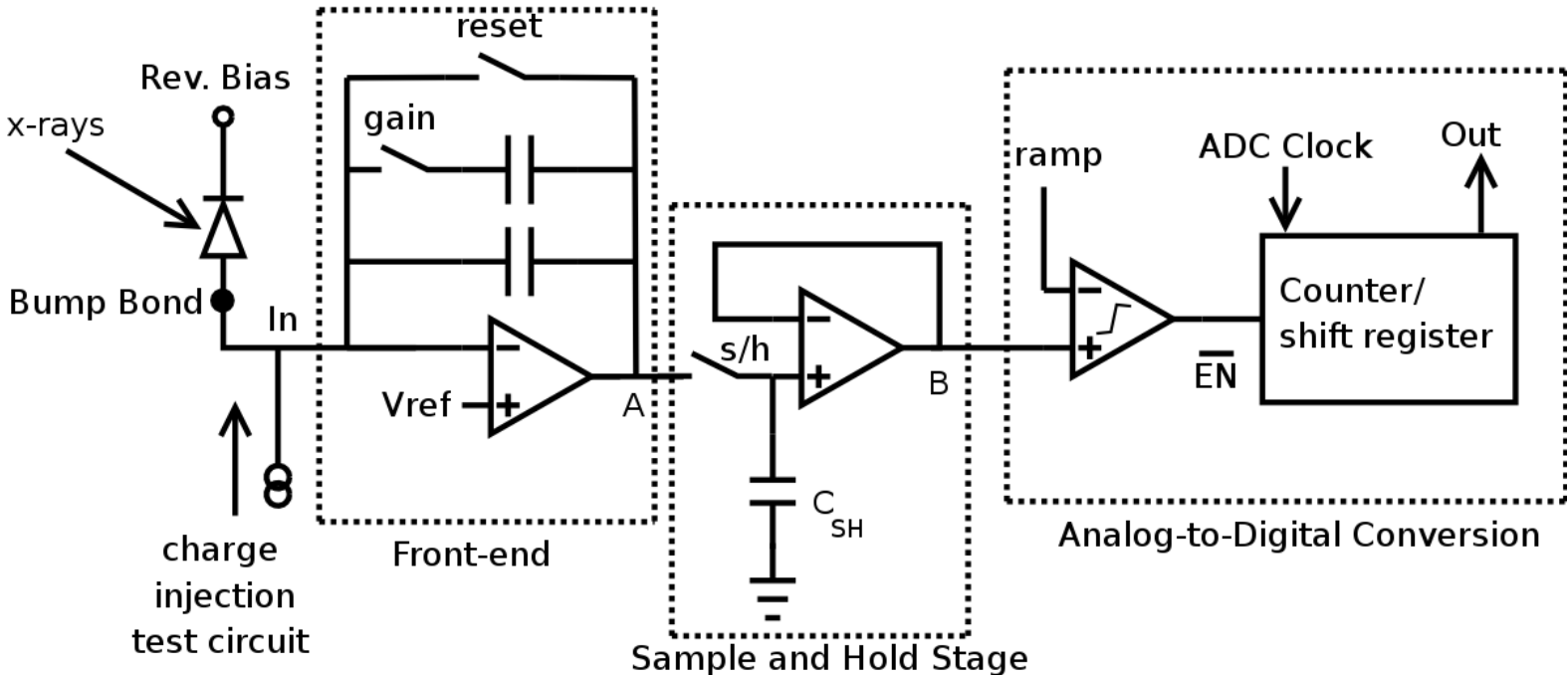
Detector



Detector

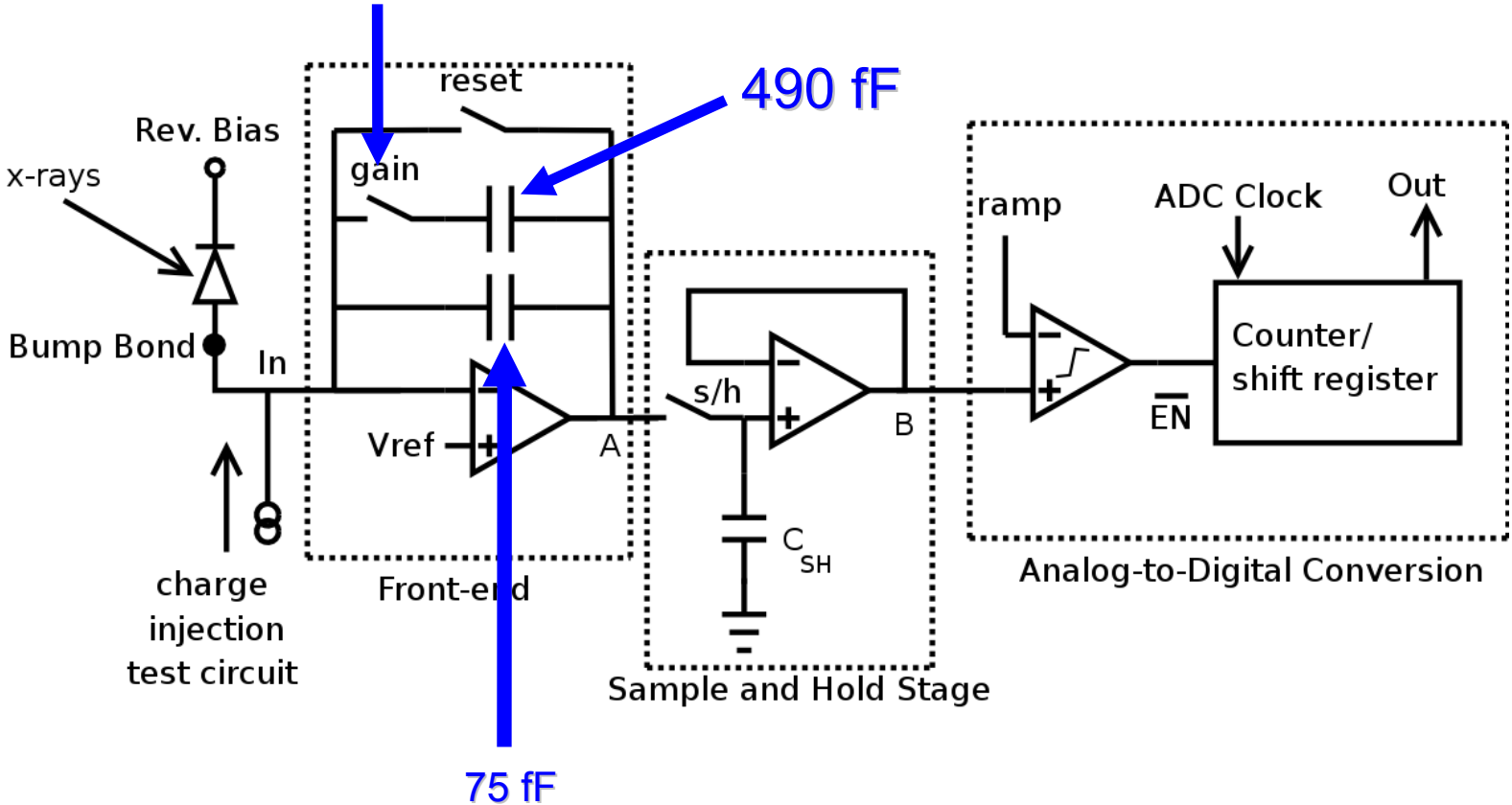


Pixel-Level Schematic



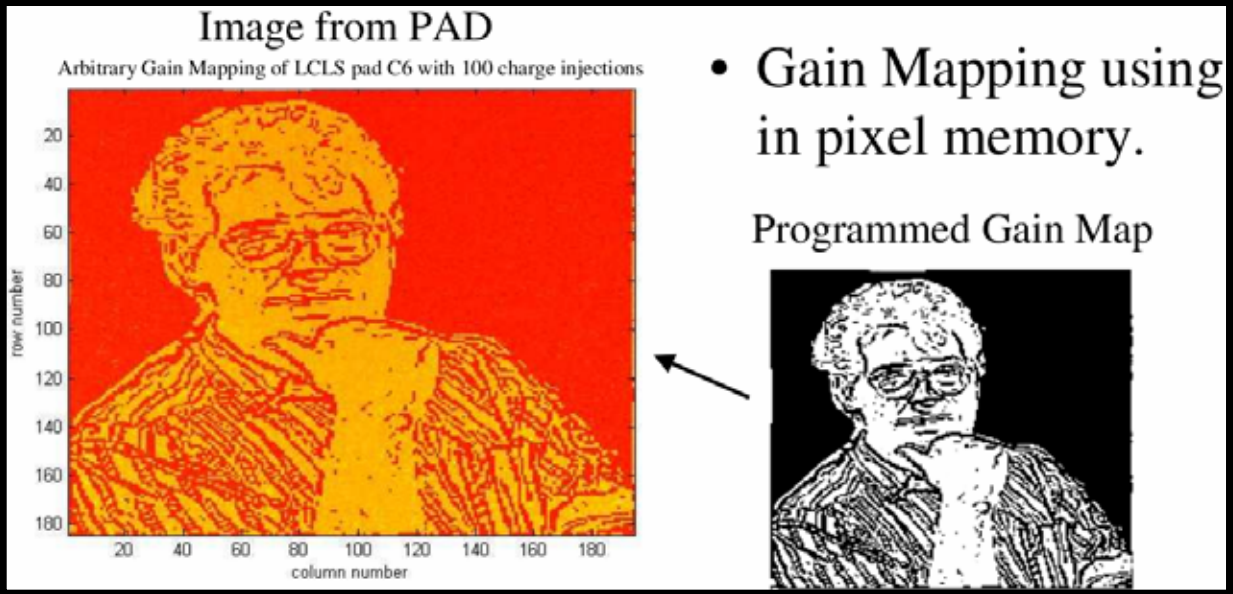
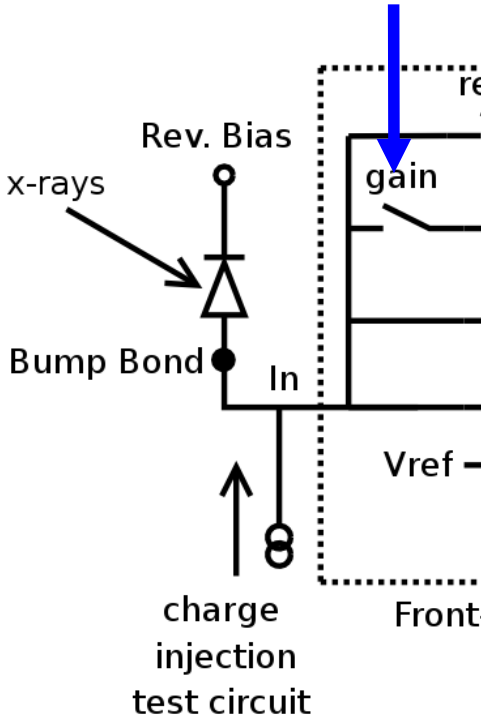
Pixel-Level Schematic

Controlled by 1-bit programmable pixel memory



Pixel-Level Schematic

Controlled by 1-bit programmable pixel memory



- Gain Mapping using in pixel memory.

Programmed Gain Map

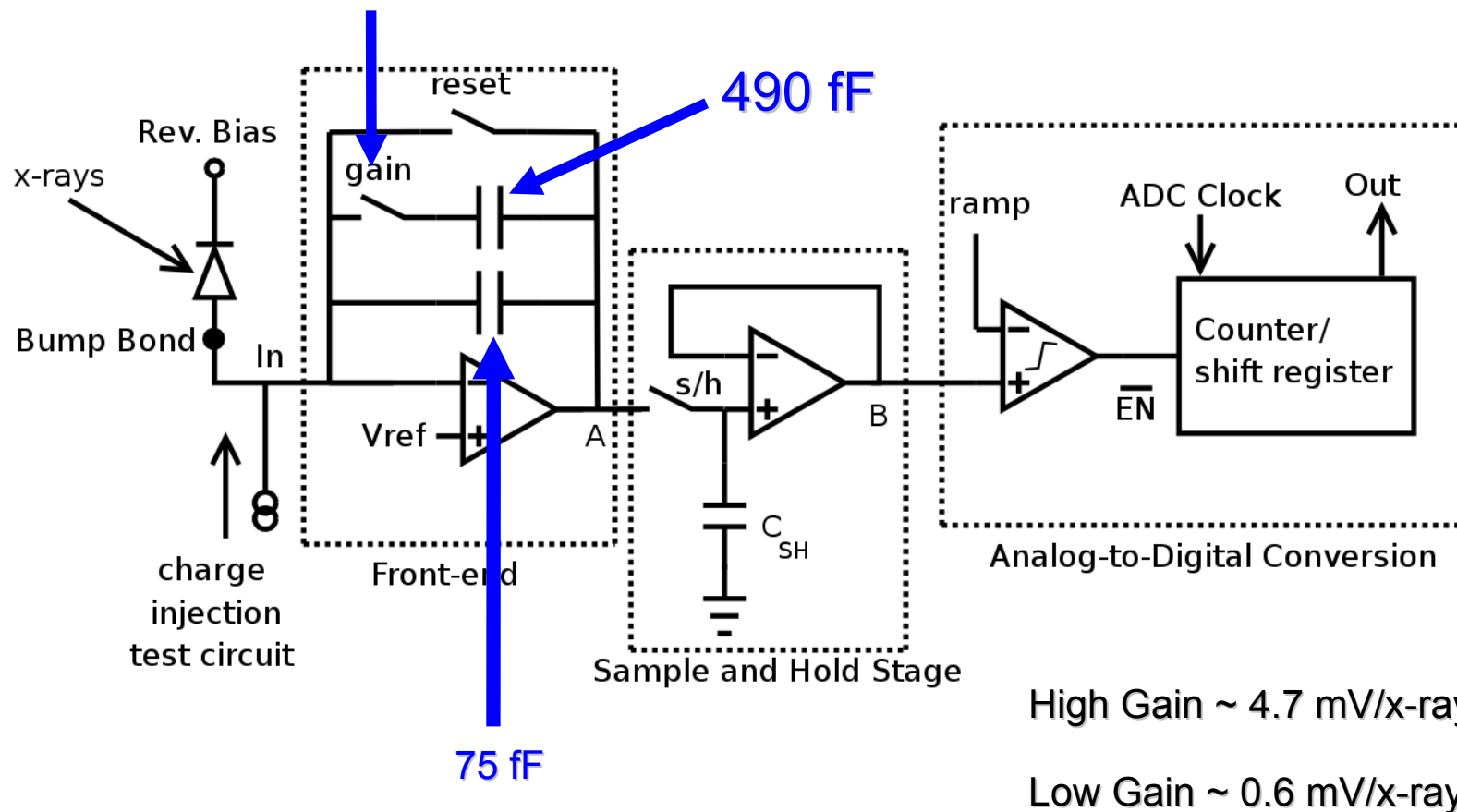


75 fF

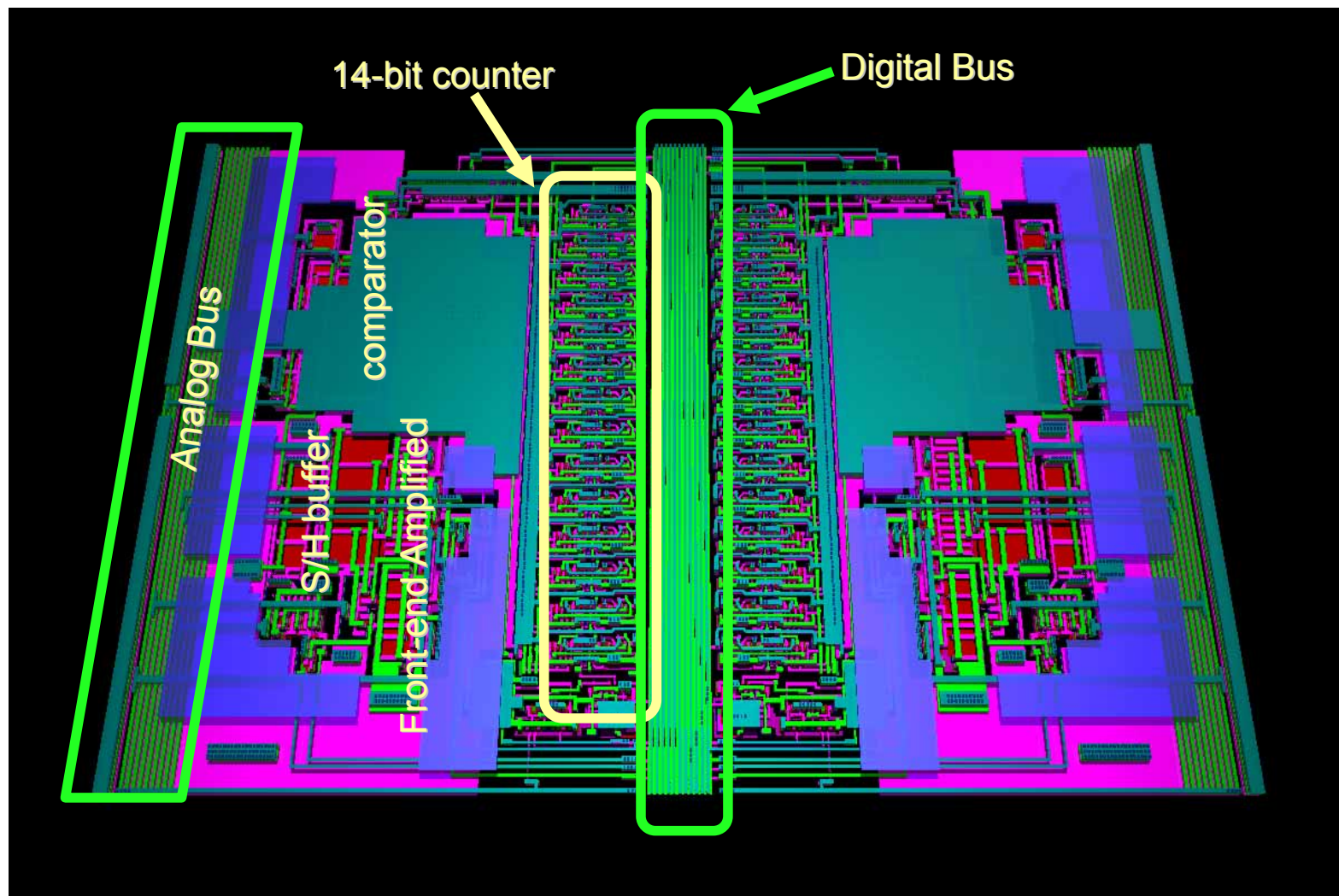


Pixel-Level Schematic

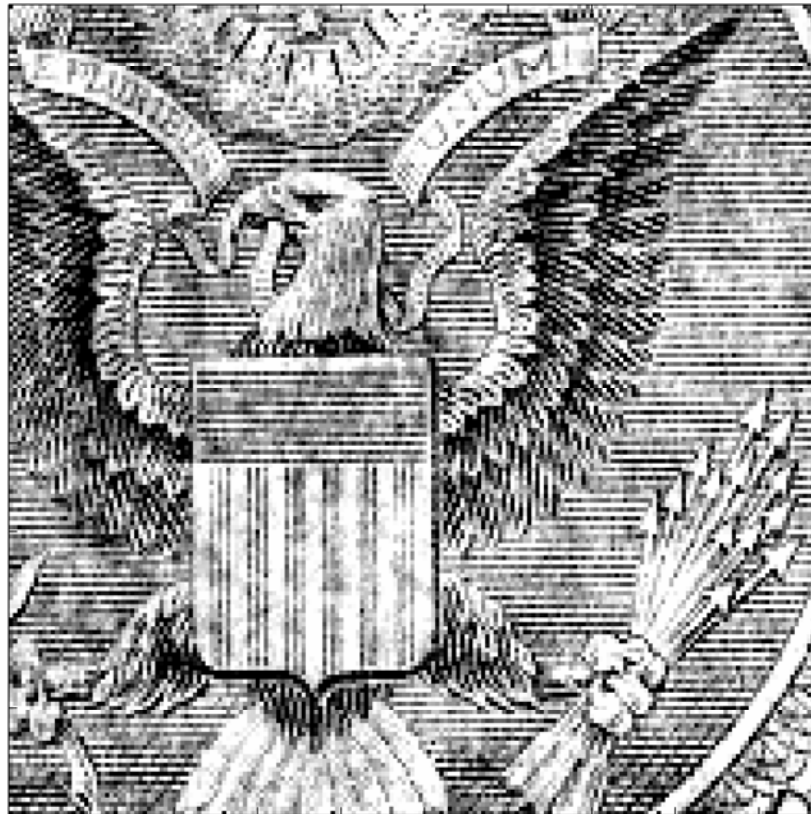
Controlled by 1-bit programmable pixel memory



Pixel Level Layout (2 pixels mirrored)



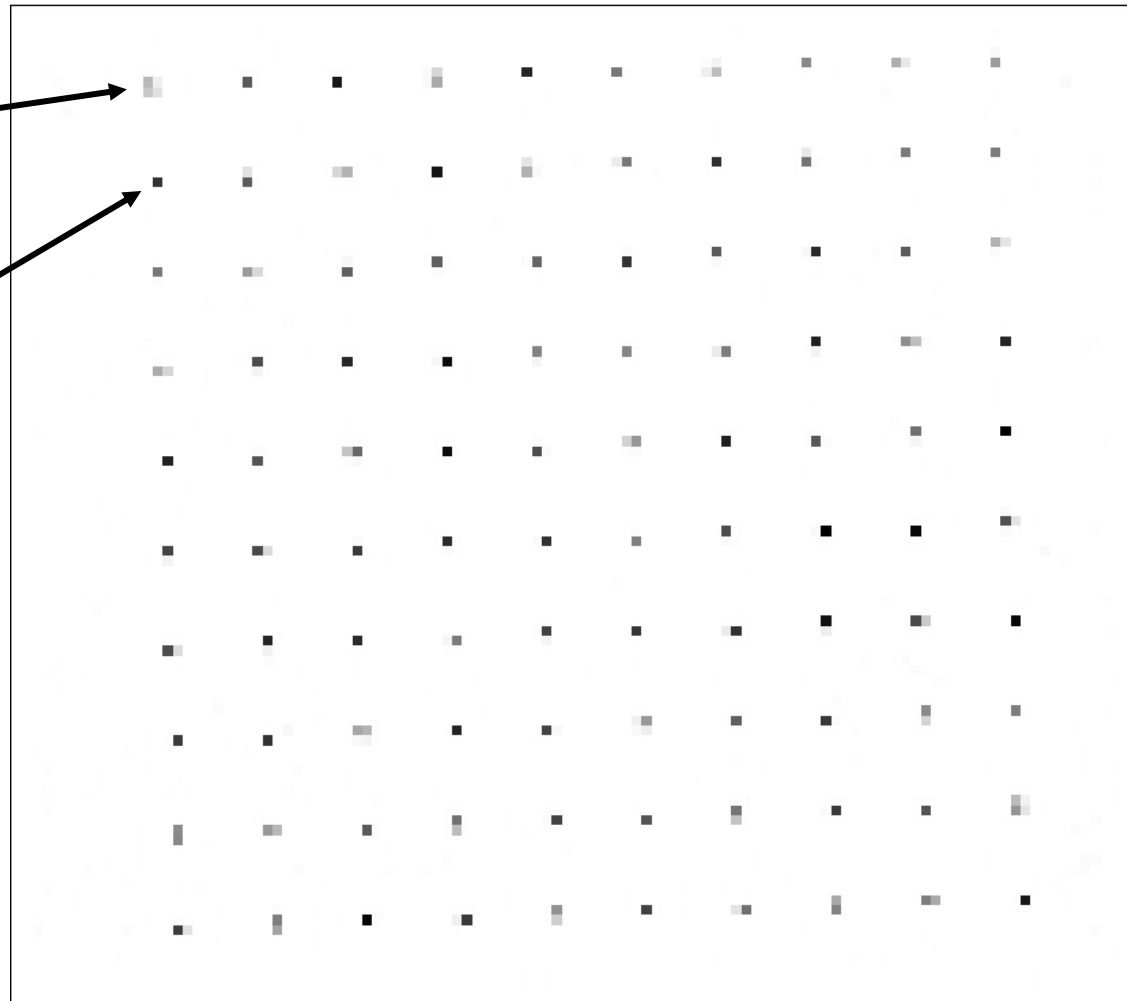
Example Radiograph of a Dollar Bill



Pinhole Mask Measured on a section of the PAD

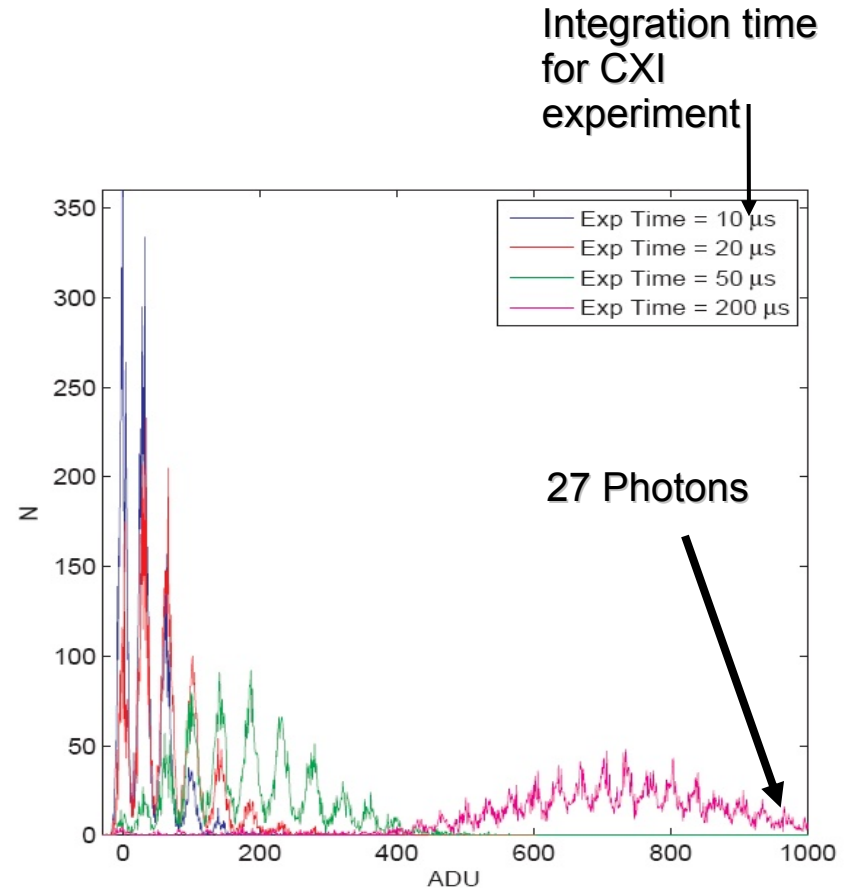
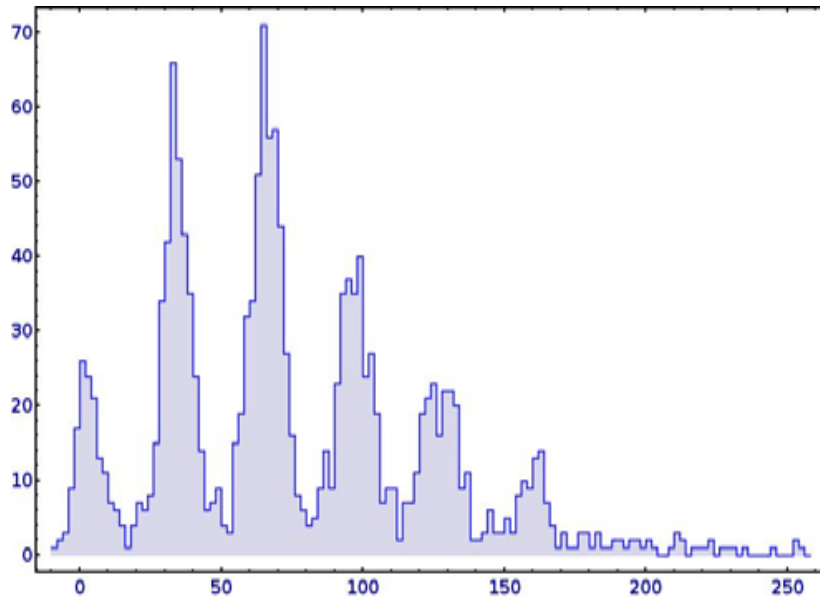
Pinhole overlaps pixel boundaries

Pinhole 'centered' on pixel



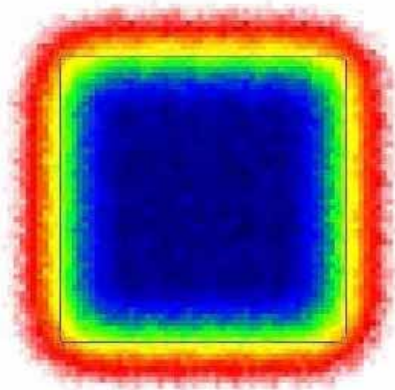
Single Photon Detection

(pinhole illuminated)

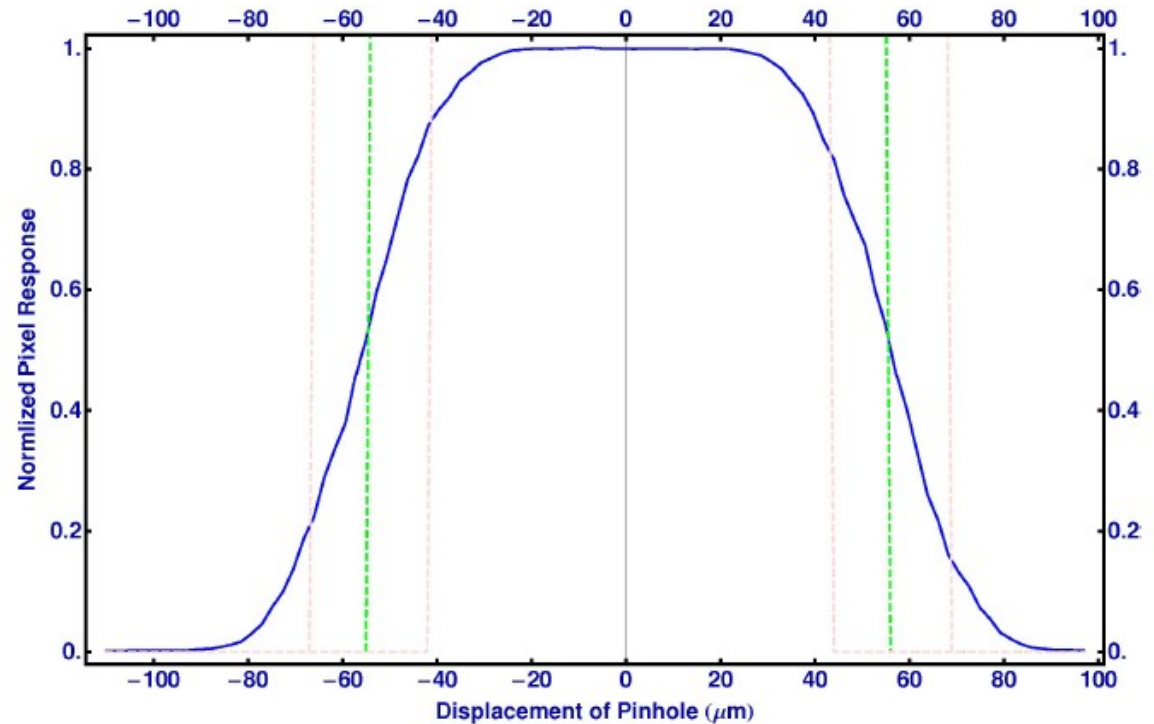


Pinhole Array Spatial Resolution

Mapped with many 25 micron pinholes



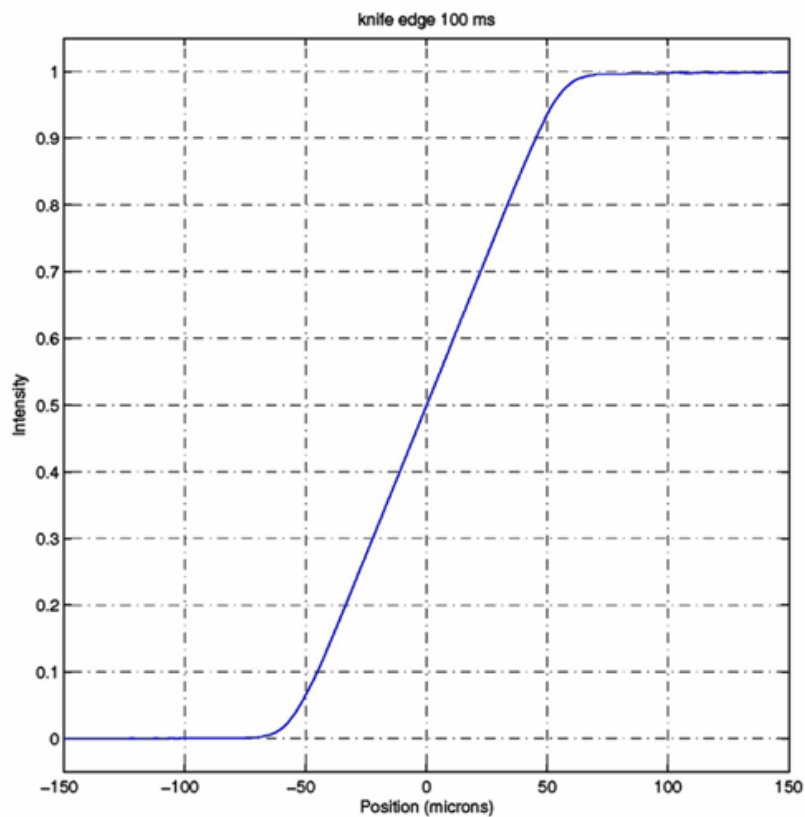
Density plot showing
uniformity of pixel response



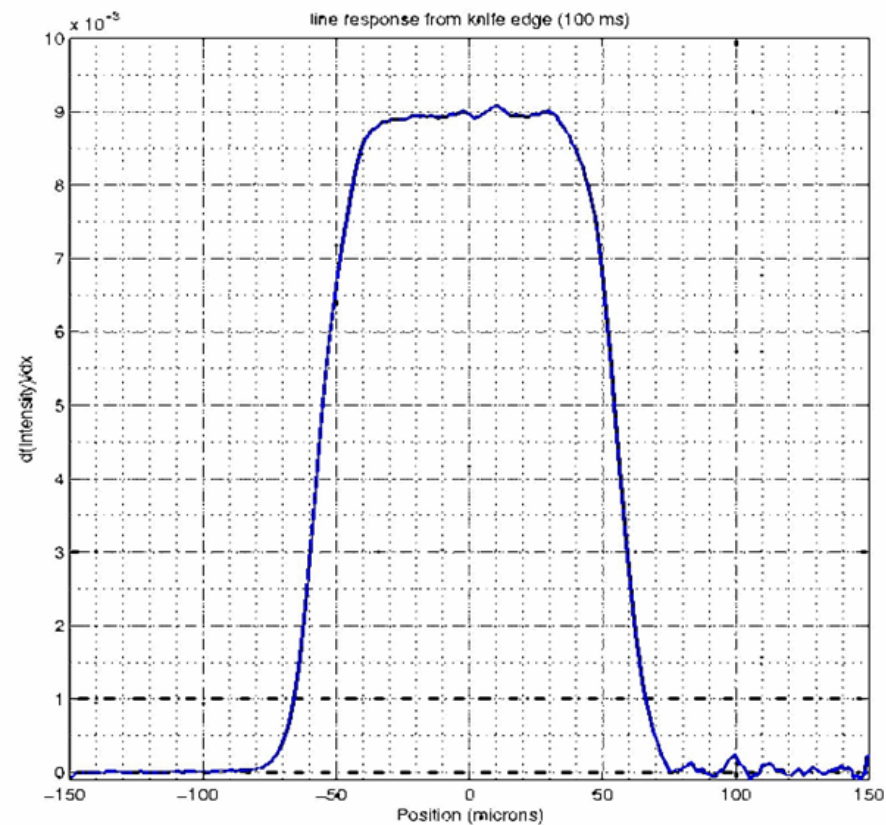
Cross Section



Knife Edge / Line Spread



Remember – Pixel width 110 microns



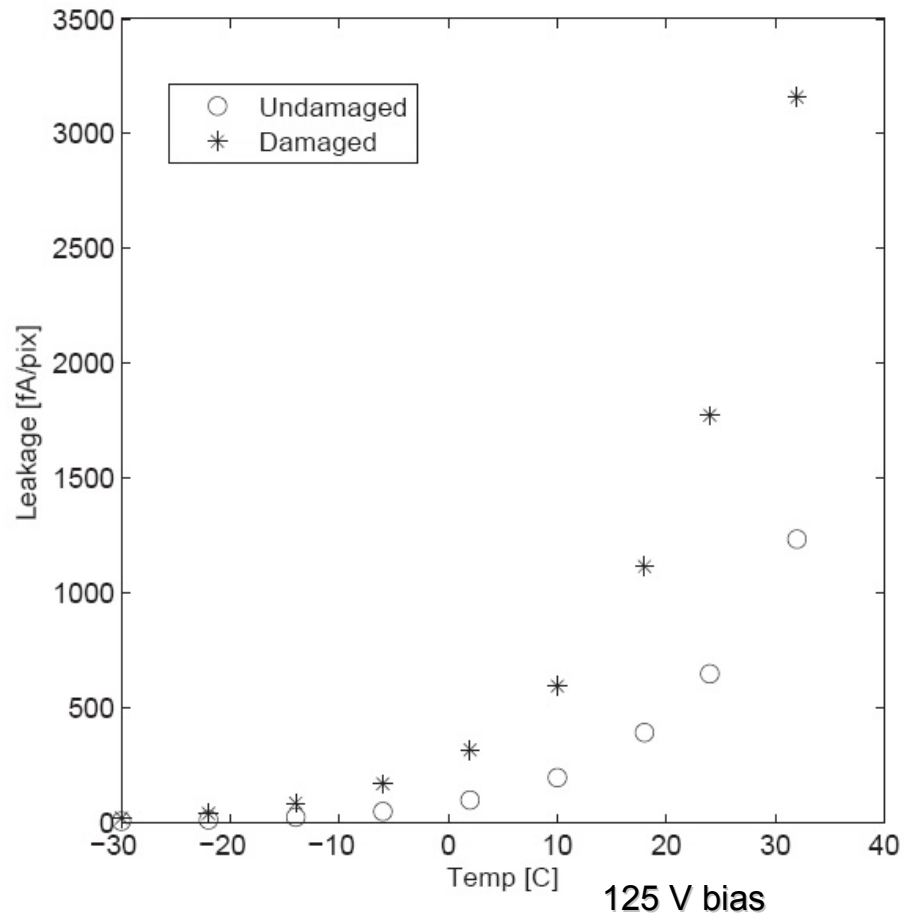
100 ms Integration Time



Radiation Dosing of Bumped Module

(75 MRad @ 8 keV)

- No apparent effect on CMOS.
- Increased leakage currents in diode.
- Single x-ray in 10 us
~35000 fA/pix (or 10 times scale shown).
- Leakage not a significant noise source.



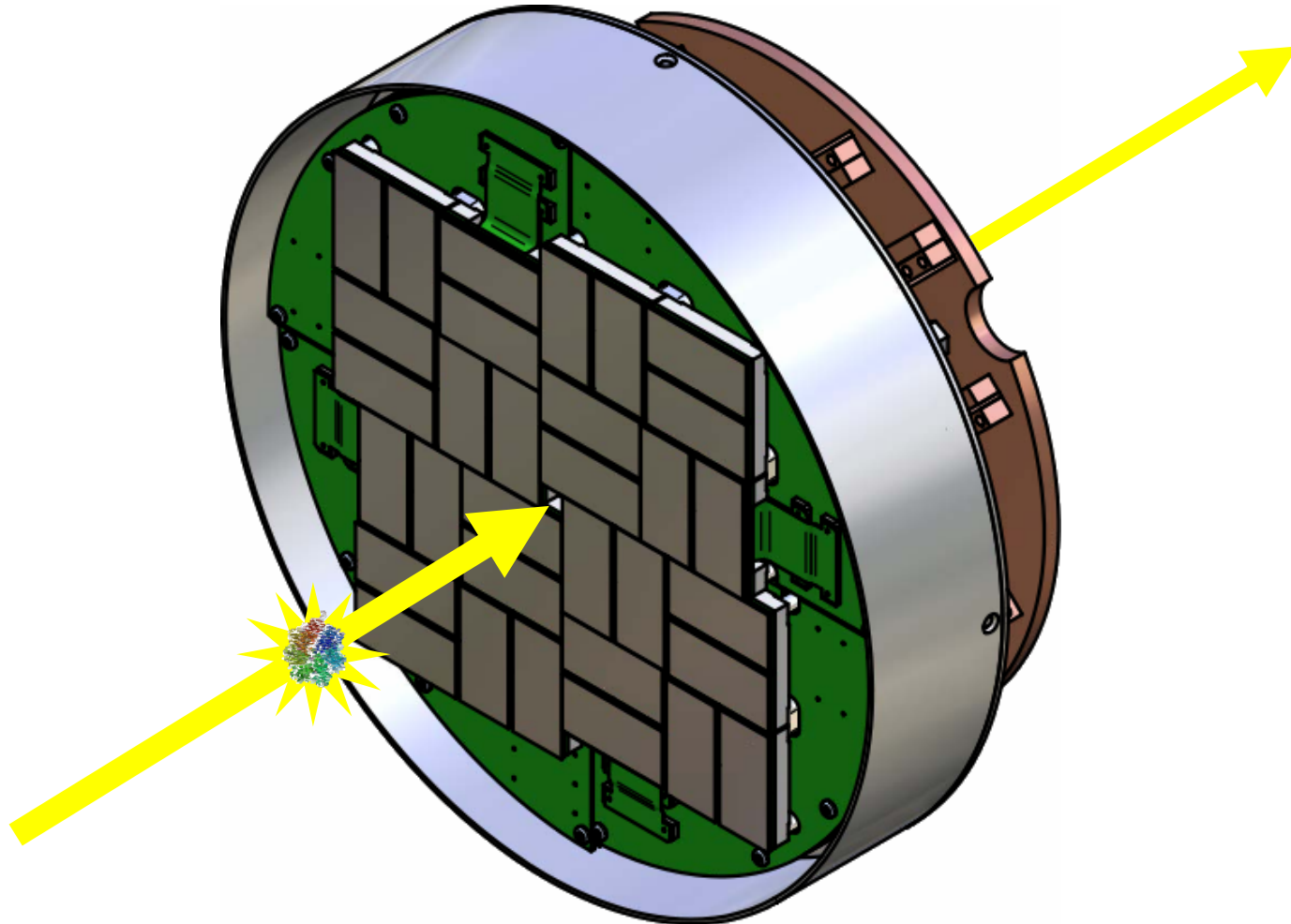
Performance of ASIC

Pixel Size	110 μm 110 μm
Array Size	185x194 pixels
Frame rate	120 Hz
Read-Noise	1000 e^- (LG) ; 350 e^- (HG)
Full-well	2,500 (LG) 300 (HG)
Quantum Efficiency^a	0.97 (8 keV); 0.89 (12 keV); 0.48 (18 keV)
Dark Current	40 fA/pix (-14 C); 700 fA/pix (18 C) $1.14 * 10^{-4}$ x-rays/ μs ; 0.002 x-rays/ μs
Bump-Bond Yield^b	0.99987; 0.99891

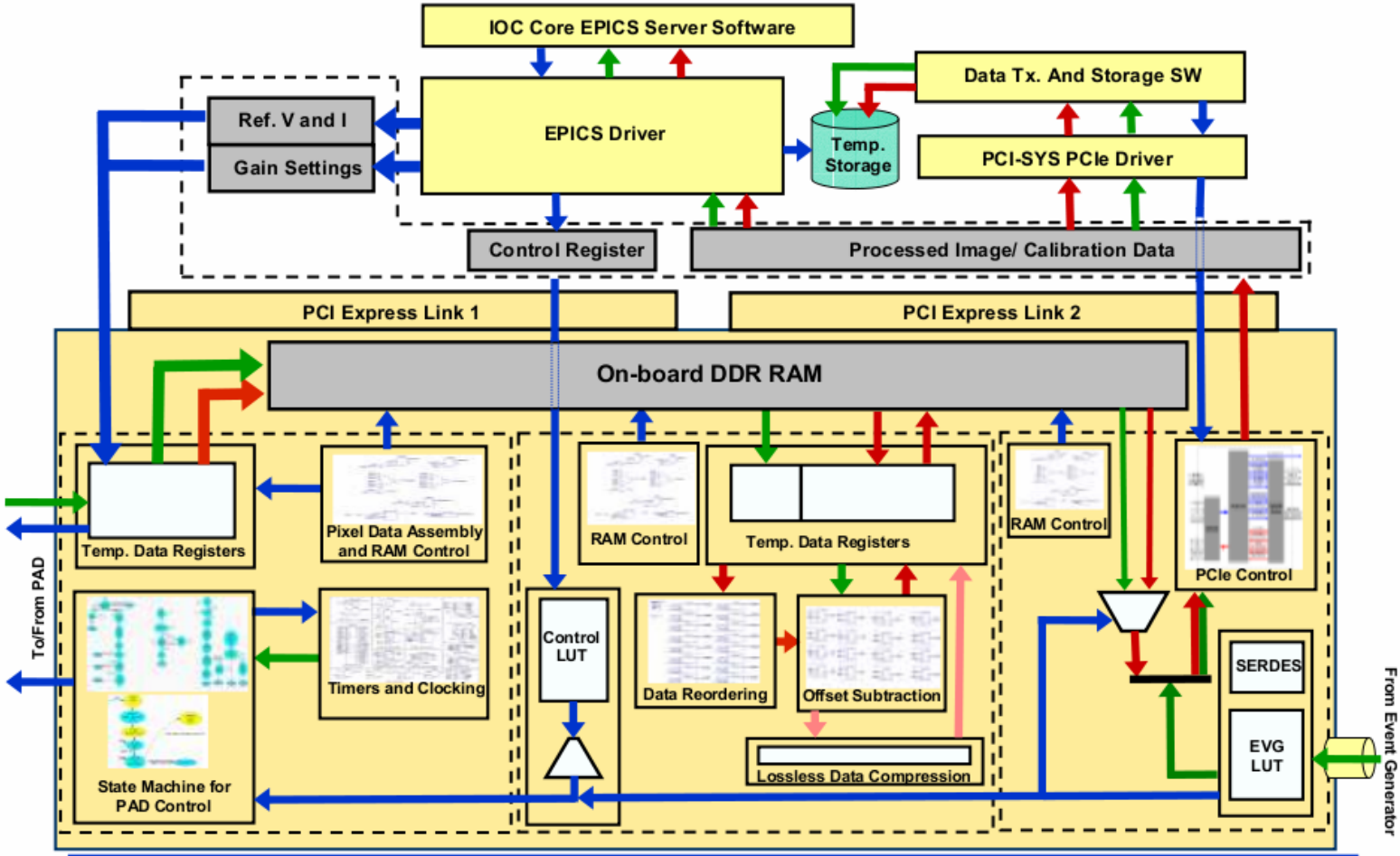
Table 1: A values in table assume 8 keV x-ray energy. ^a Calculated values. ^b Median and mean bump-yield of 16 assemblies tested. All but one module (0.987) measured bump-yields of > 0.9987 .



So, what how will this thing look?



Note: Data Acquisition System is not really covered here... but it is NOT trivial



Example 3: Mixed Mode PAD

Mixed-Mode Pixel Array Detector (PAD)

Detector Format	Multi-Mosaic of PAD Tiles
Single PAD Tile Format (ASIC)	128 × 128 Pixel
Pixel Size	150 μm × 150 μm
Framing Rate	20 Hz (continuous) / 1,000 Hz (burst)
Readout Time	< 1 ms
Read Noise	0.3 X-Ray [12 keV]
Well Capacity	2.6 × 10 ⁷ X-Ray [12 keV]/pixel
Maximum Flux	1.0 × 10 ⁸ X-Ray [12 keV]/s/pixel

- Developing the prototype has been a collaboration between Cornell and Area Detector Systems Corp. (ADSC).
- Commercialization is dependant on ADSC.



Mixed Mode PAD has Enormous Span

- Standard Dynamic Range Definition:

$$\text{Dynamic Range} = \frac{\text{Well Depth}}{1 \sigma \text{ Level}}$$

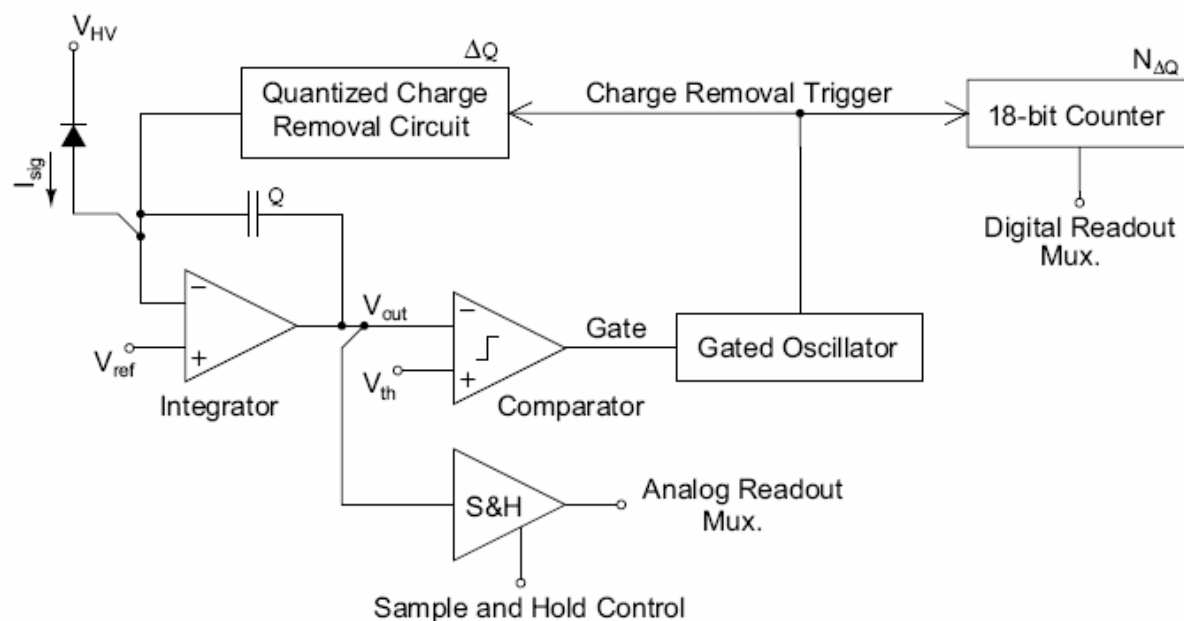
- What happens when the integration time is short?
 - e.g. in 10 ms a detector flux limited to 10^6 x-rays/s/pixel cannot measure more than 10,000 x-rays/pixel.
- Alternative Dynamic Range Definition:

$$\text{Effective Dynamic Range} = \frac{\text{Detector Flux Limit} \cdot \text{Exposure Duration}}{1 \sigma \text{ Level}}$$

- Mixed-Mode PAD 10^8 x-rays/s/pixel Flux Limit
→ Mixed-Mode PAD excels at fast exposures.



Example 3: Mixed Mode PAD



1. Photocurrent (I_{sig}) collects in the **integrator**.
2. The **integrator output** (V_{out}) slews towards ground.
3. When $V_{out} < V_{th}$, the **comparator** activates a **gated oscillator**.
4. Each oscillator cycle **removes a fixed quantity of charge** (ΔQ) from the integrator and **increments an in-pixel counter** ($N_{\Delta Q}$).



Example 3: Mixed Mode PAD

Custom in-pixel signal processing → great flexibility in PAD application.

Two methodologies implemented prior to the Mixed–Mode PAD:

- **Photon Integrating PADs:**

Collect x-ray signal in an integrator, digitized post acquisition.

- **Photon Counting PADs:**

Shape, discriminate, and count x-ray pulses.

	Mixed–Mode PAD	Cornell 100 × 92	Medipix–2	Pilatus
PAD Method	Mixed	Integrating	Counting	Counting
Pixel Size [μm^2]	150 × 150	150 × 150	55 × 55	172 × 172
Read Noise [10 keV x-rays]	0.4	~ 2.6	< 1	< 1
Frame Rate [Hz]	20, 1,000	1, 10^6	~1,000	12.5 (6M), 300 (100k)
Well-Depth [10 keV x-rays/pixel]	~ 2×10^7	~ 1.7×10^4	~ 1.6×10^4	~ 10^6
Maximum Flux [10 keV x-rays/pixel/s]	> 1×10^8	10^{12}	2×10^6	< 8×10^6

Red → 😊 Blue → ☹️

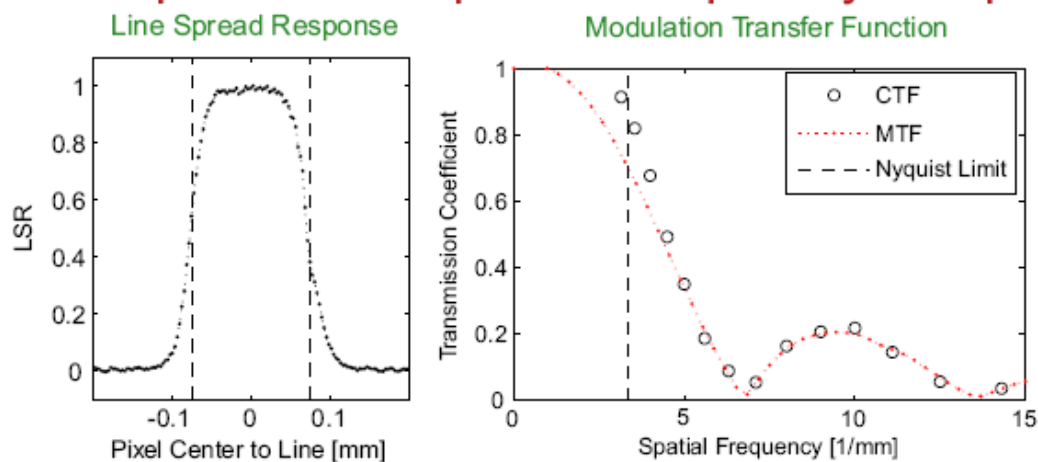
The Mixed–Mode PAD combines aspects of both these approaches to create a device that is *uniquely suited to synchrotron science*.



Example 3: Mixed Mode PAD



Detector Spatial and Spatial Frequency Response



Single image response is dominated by discrete sampling.

$\sim 45 \mu\text{m}$ charge sharing region.

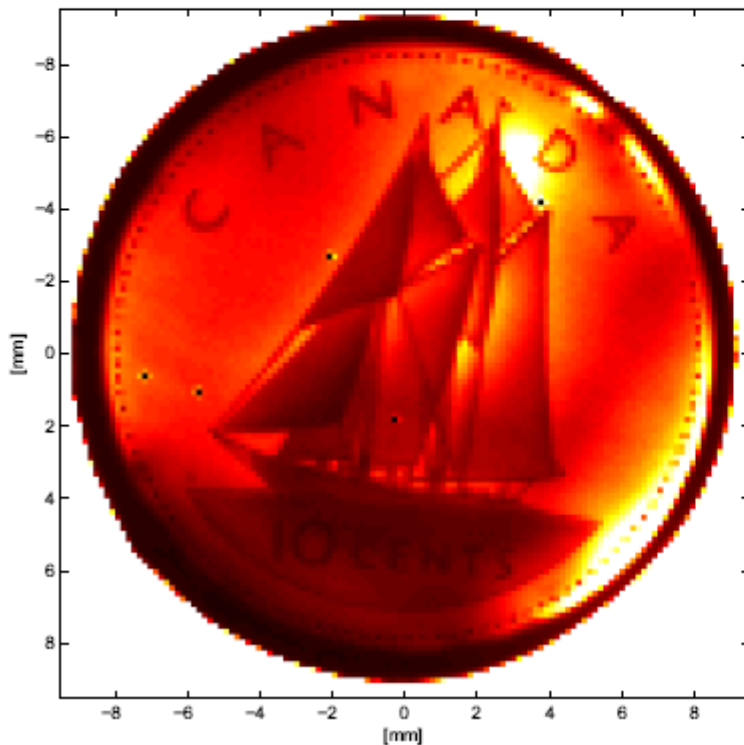


Example 3: Mixed Mode PAD

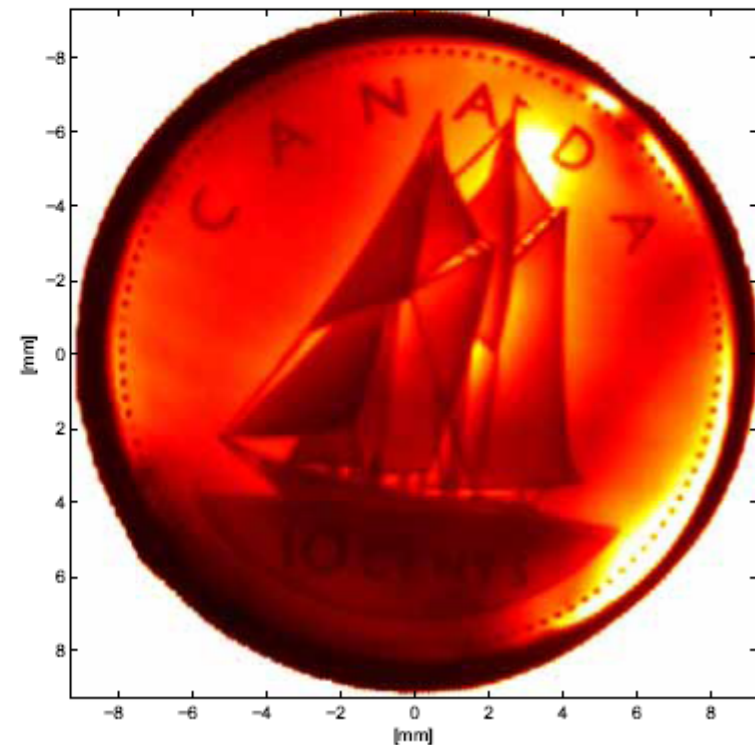
X-Ray Radiograph of a Canadian Dime

(One side filed off to eliminate image superposition.)

Single Image

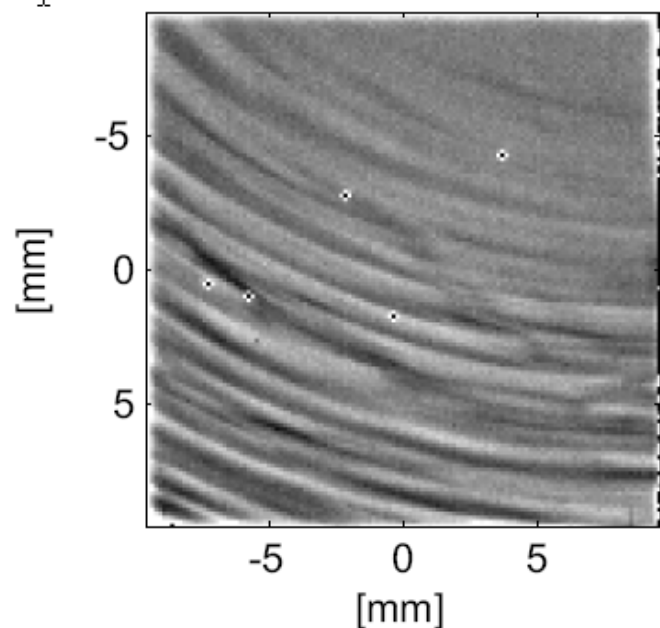


Finely Sampled Image



Spatial Distortion

Thick detector layer → **all** PADs are subject to spatial distortion.



- Caused by lateral fields within the detector layer → doping inhomogeneities.
- Effectively some pixels are bigger than others!



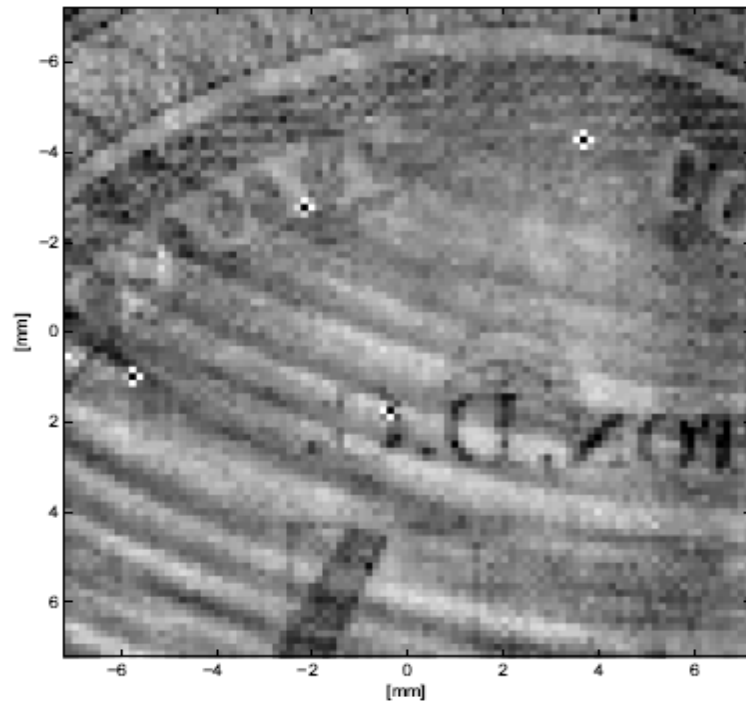
• Donor Dopant



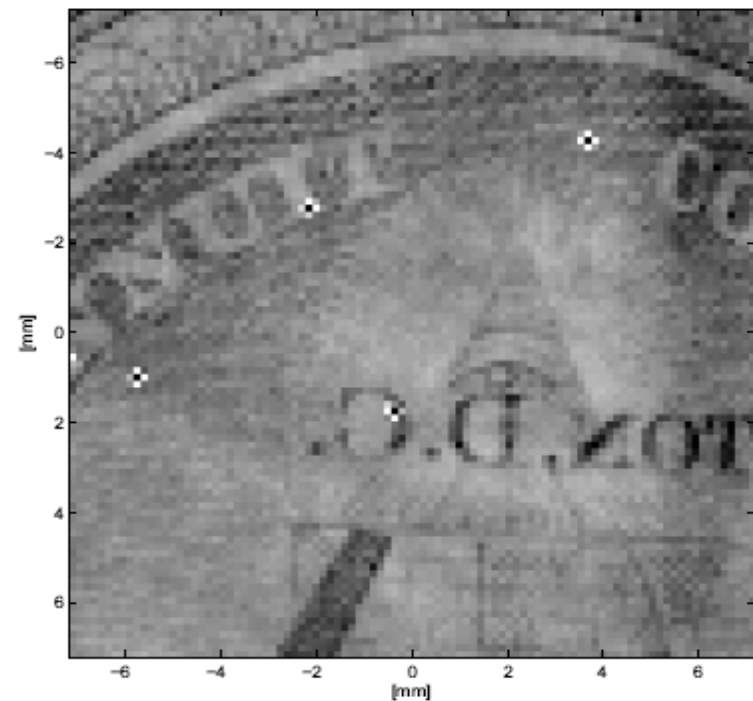
Spatial Distortion

Distortion can be Corrected in Post-processing

Raw



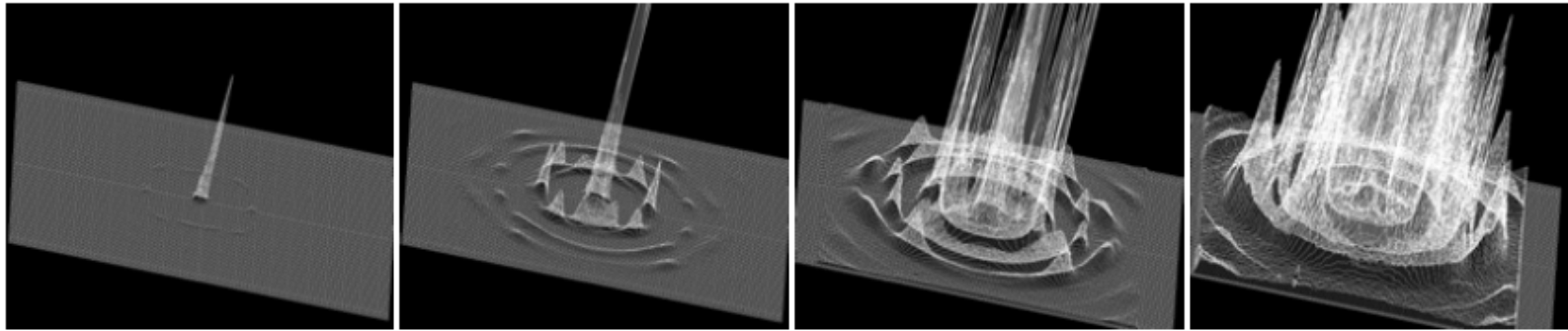
Corrected



● Signal preserving correction.

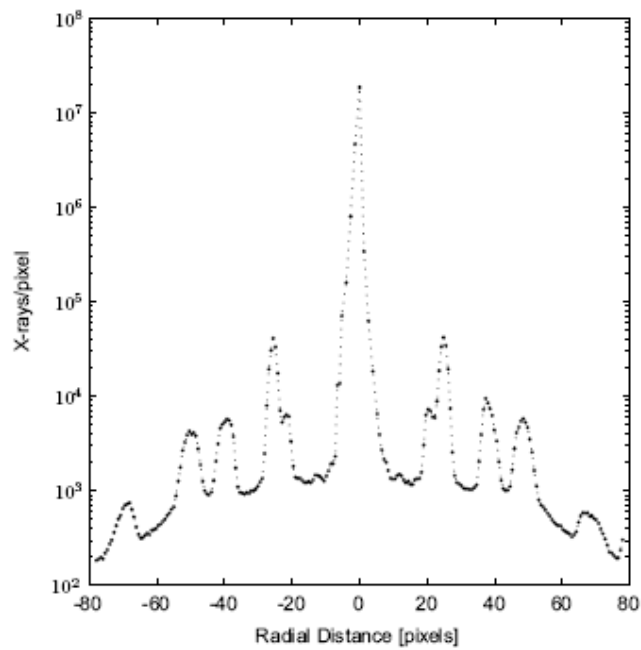


Wide Angle Diffraction from Aluminum



→ → Increasing intensity scale → →

Diffraction Line Profile

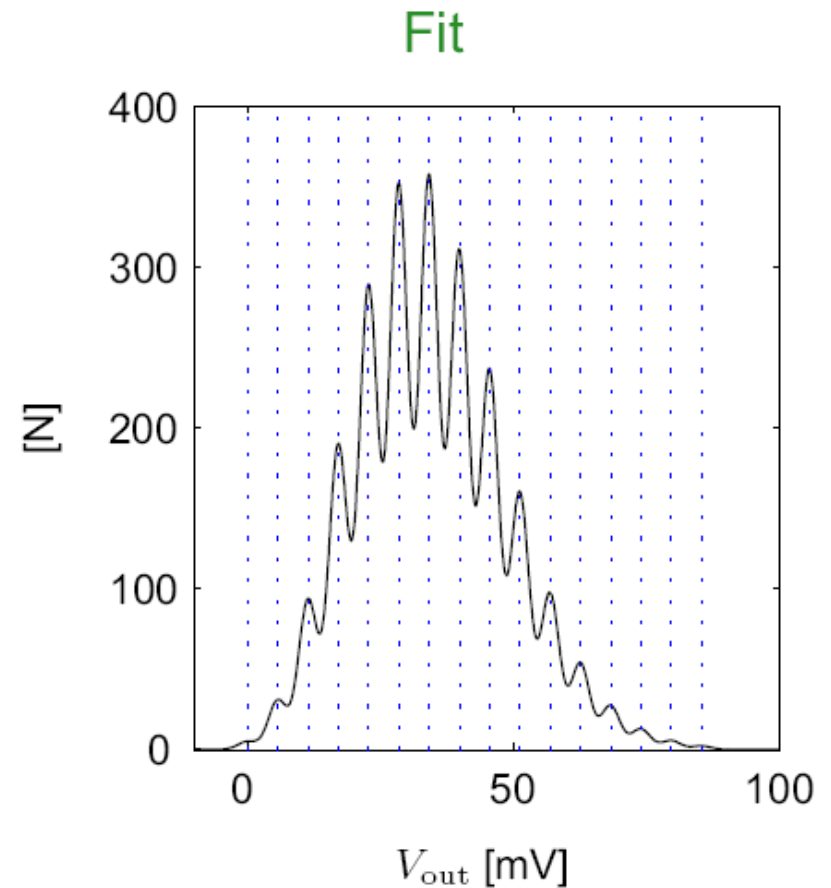
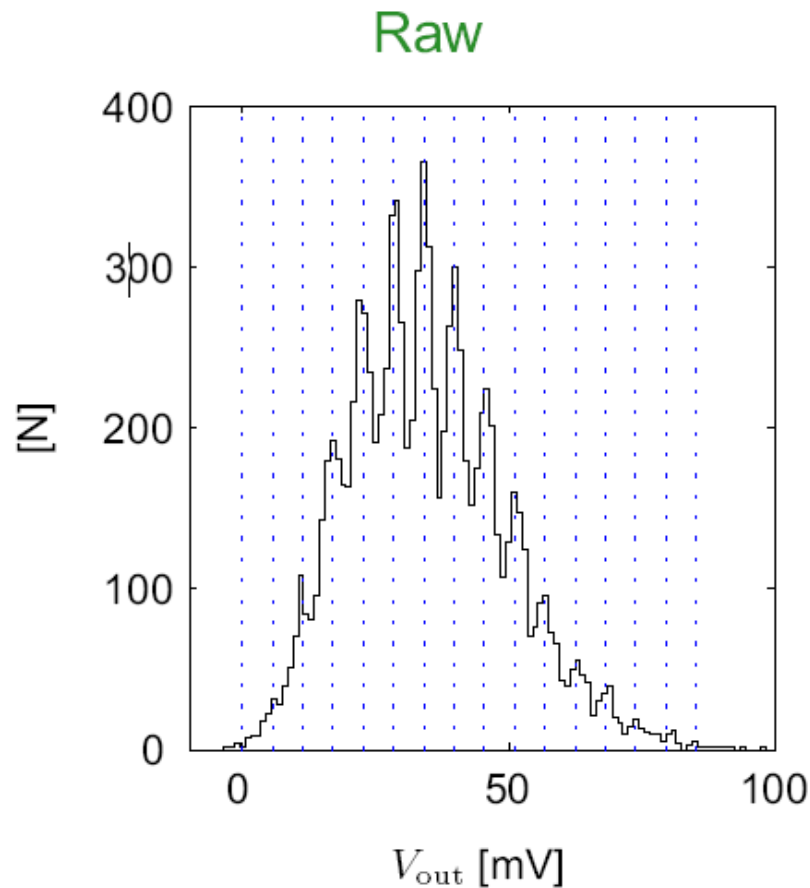


- Single image, 1 second exposure of Al sheet.
- Peaks differ by a $\sim \times 25,000!$
- *A larger detector would reveal even more dynamic range.*



Single Photon Sensitivity

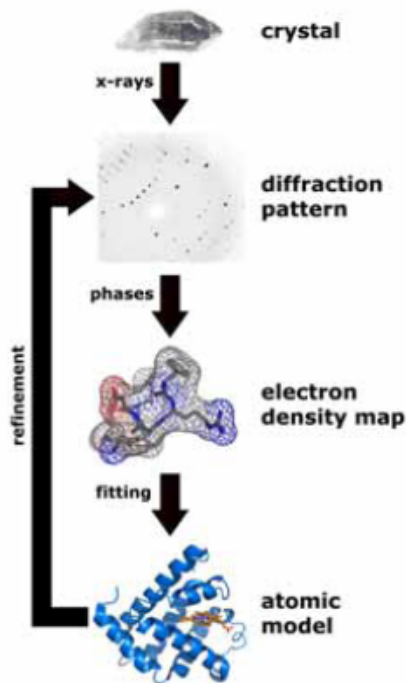
Single Pixel Poisson Spectra - Cu K_{α} (8.05 keV)



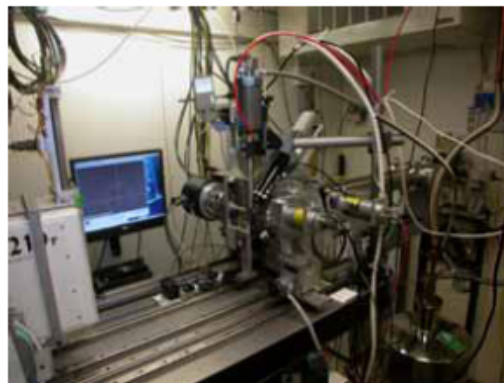
Protein Crystallography

First Mixed-Mode PAD Experiment: Macromolecular Protein Crystallography

- Macromolecular Crystallography uses x-ray diffraction to determine the atomic structure of complicated biological molecules, e.g. proteins and viruses.
- Diffraction reveals the Fourier Transform of the molecule's electron density map.

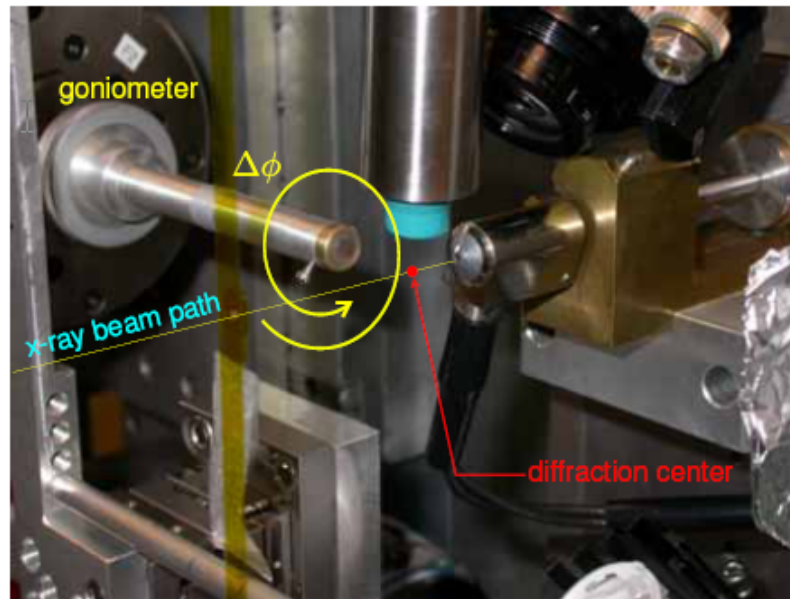


F2 Beamline at CHESS



Protein Crystallography

Canonical Data Taking Method



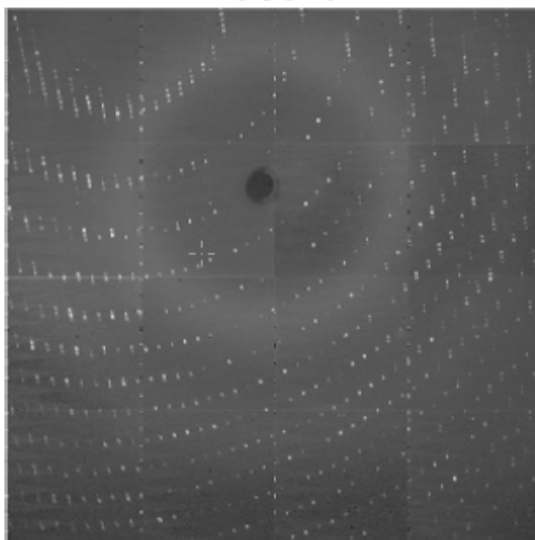
- Need to sample enough of the crystal diffraction pattern to reconstruct the protein's electron density map.

- Sample is rotated through a **large angle** ($\Delta\phi = 0.5\text{--}2.0$ deg is typical) while detector acquires a single **long exposure** (≥ 10 s often).
- Process is repeated until enough of the diffraction pattern is collected to reconstruct the protein's electron density map.



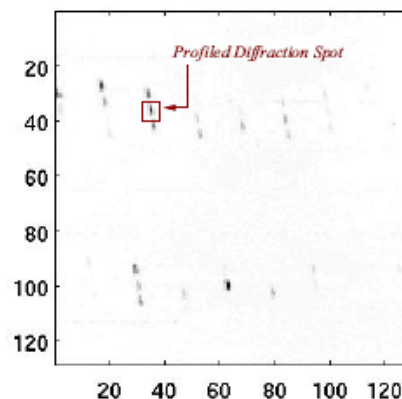
Protein Crystallography

Thaumatococcus
Mosaic

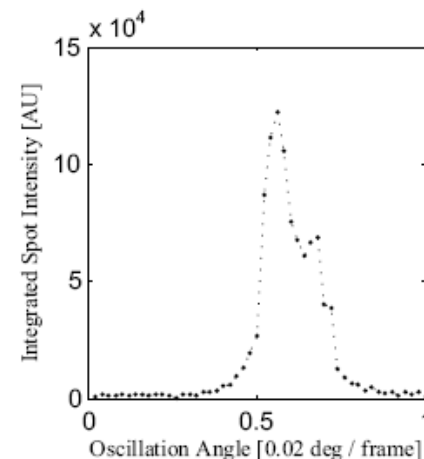


Thaumatococcus Fine ϕ -slicing

Canonical Diffraction



Diffraction Spot Profile



Advantages of ϕ -slicing

- Full data set can be taken in a **single, continuous rotation**
→ **faster data collection** and **eliminates systematic errors**.
- **Reveals new information** about the crystal.
- **Reduces background** in spot intensity measurement.



Cornell PAD Group

- **Actively working on PAD projects at Cornell:**
 - Marianne Hromalik
 - Lucas Koerner
 - Mark Tate
 - Kate Green
 - Darol Chamberlain
 - Sol Gruner
- **Recent Past:**
 - Dan Schuette

